LAWRENCE
LIVERMORE
NATIONAL
LABORATORY

LLNL-JRNL-814027

NanoSIP: NanoSIMS applications for microbial biology

J. Pett-Ridge, P. K. Weber

August 27, 2020

Methods in Molecular Biology

Disclaimer

NanoSIP: NanoSIMS applications for microbial biology

Jennifer Pett-Ridge and Peter K. Weber

Running Head: NanoSIMS for Microbial Biology

Jennifer Pett-Ridge
Lawrence Livermore National Lab, Physical and Life Science Directorate
7000 East Avenue
Livermore, CA 94550
pettridge2@llnl.gov

Peter K. Weber
Lawrence Livermore National Lab, Physical and Life Science Directorate
7000 East Avenue
Livermore, CA 94550
weber21@llnl.gov

LLNL-JRNL-814027

Abstract

High-resolution imaging with secondary ion mass spectrometry (nanoSIMS) has become a standard method in systems biology and environmental biogeochemistry and is broadly used to decipher ecophysiological traits of environmental microorganisms, metabolic processes in plant and animal tissues, and cross-kingdom symbioses. When combined with stable isotope-labelling –an approach we refer to as *nanoSIP*— nanoSIMS imaging offers a distinctive means to quantify net assimilation rates and stoichiometry of individual cell-sized particles in both low- and high-complexity environments. While the majority of nanoSIP studies in environmental and microbial biology have focused on nitrogen and carbon metabolism (using ^{15}N and ^{13}C tracers), multiple advances have pushed the capabilities of this approach in the past decade. The development of a high-brightness oxygen ion source has enabled high resolution metal analyses that are easier to perform, allowing quantification of metal distribution in cells and environmental particles. New preparation methods, tools for automated data extraction from large data sets, and analytical approaches that push the limits of sensitivity and spatial resolution have allowed for more robust characterization of populations ranging from marine archaea to fungi and viruses. NanoSIMS studies continue to be enhanced by correlation with orthogonal imaging and 'omics approaches; when linked to molecular visualization methods, such as in situ hybridization and antibody labeling, these techniques enable *in situ* function to be linked to microbial identity and gene expression. Here we present an updated description of the primary materials and methods used for nanoSIP, with an emphasis on recent advances in nanoSIMS applications, key methodological steps and potential pitfalls.

Key Words: nanoSIMS, isotope assimilation, metal imaging, single cell biology, sample preparation, SEM, TEM, FIB, FISH, O^- ion source

1. Introduction

Understanding biological exchanges at the single cell scale, especially in complex systems, is one of the grand challenges of microbial ecology and systems biology. This challenge includes characterizing cell-cell interactions, linking phylogenetic identity to ecophysiology for uncultured organisms, and quantifying rates of elemental transfers within and between cells and their surrounding matrix. Recent advances in 'omics techniques have enabled unprecedented access to gene transcripts, metabolites and proteins, but rarely at the level of individual cells or mineral particles. These data have also enabled insights into the genomic potential of uncultured organisms that exist in complex systems, however, quantitative measures of metabolic functions of these organisms and within-population variability remain largely untested. Isotope tracing techniques are unique in their ability to identify *in situ* ecophysiology of microorganisms and biogeochemical exchanges, making them some of the most powerful techniques in microbial ecology[1-6]. Amongst these approaches, the development of high-resolution secondary ion mass spectrometry[7], specifically with a CAMECA NanoSIMS 50 and later the 50L, has opened up new capabilities for taking on the challenge of single cell scale isotope imaging and has become a standard method for assessing *in situ* metabolic activity.

Nanoscale secondary ion mass spectrometry (nanoSIMS) [7] is a quantitative imaging technique where a high-energy primary ion beam is used to sputter small volumes of sample surface material, generating secondary ions that are used to create atomic or molecular ion maps. Its high lateral resolution (~ 50 nm) and parts per million to high parts per billion detection limit enables *in situ* characterization of isotope enrichment and elemental composition at the single

cell level. The NanoSIMS 50 and 50L (CAMECA, Gennevilliers, France) can image 5 - 7 elements or isotopes simultaneously; additional species can be imaged using a magnetic peak switching approach[8]. These characteristics enable mapping of trace element and isotopic variations with submicron-scale resolution, including in subregions of individual cells (**Fig. 1, 2, 3**). Measurement precision in submicron regions is typically 1 % for isotope ratios; higher precision can be achieved in larger volumes. As such, nanoSIP studies typically involve isotope or rare element labeling, although microscale imaging of naturally occurring elemental or isotope fractionation patterns is possible[9, 10].

NanoSIMS was first intensively applied to meteoritic material [11], and in the early 2000's to biological materials ranging from cell membranes to bacteria, eukaryote symbionts, archaea, cyanobacteria, spores, biominerals and soils [12-28]. Interest in nanoSIMS applications for microbial ecology, cell biology and environmental science has grown quickly between that period and the present, with multiple CAMECA nanoSIMS instruments in use specifically for these applications. Today, nanoSIMS analysis is a well-accepted technique, and has been discussed in over 1000 publications from many disciplines. Multiple literature reviews have been published that focus on applications including soils[28, 29], biofilms[30], marine ecology[31], cell metabolism[32], plant elemental distribution[33], the combination of nanoSIP with fluorescent in situ hybridization (FISH)[34], general biological applications[35-37] and cell membranes[38]. An updated list of nanoSIMS literature in environmental biology and cell biology may be found at https://www.cameca.com/products/sims/nanosims[39]. In this updated version of our 2012 chapter[40], we discuss advances in nanoSIMS analysis techniques, new applications, and methodologies that are becoming standardized.

Recent Developments in nanoSIMS Systems Biology Research

With nanoSIP, metabolic activities of single microbial and eukaryotic cells and their symbionts can be tracked by imaging natural isotopic and elemental composition or isotope distribution after stable isotope probing [40]. Most nanoSIP environmental microbiology studies have targeted nitrogen and carbon metabolism (using ^{15}N and ^{13}C enriched tracers) (e.g. [31, 41-43]), but a growing number discuss patterns of sulfur, phosphorous, and metals (e.g. [44-49]) or use D_2O as a means to track active cells [50, 51]. While many of the earliest nanoSIP microbiology studies were focused on aquatic bacterial and archaeal communities [18-20, 52], and ^{13}C and ^{15}N fixation in diazotroph cultures such as *Trichodesmium spp.*[23] (**Fig. 1**) and *Anabaena oscillarioides* (**Fig. 2**) [25], recent years have brought a large expansion in the types of microbial study systems. These include: methane producers and consumers in aquatic and industrial waste treatment systems ([18, 53-58], many types of symbionts[43, 59-61], and taxa found in the human gut microbiome[62] and insect gut[63, 64]. NanoSIMS imaging has proved particularly useful for studies of elemental exchanges between symbionts, and has been applied in sponges and corals[65-70], algal-bacterial interactions[71-73], ant-plant-fungus interactions[74] and microbial mat studies of multi-functional group interactions[75].

In the past decade, nanoSIP approaches have been used to support a systems-level understanding in a substantially expanded pool of study systems, including plants, fungi, soils and viruses. In plants, elemental distributions of Zn, Cd, Fe, Mg, K, Cu, As, Si and U have been mapped at the cellular and subcellular scale as a means to understand patterns of hyperaccumulation, toxicity and metabolism (reviewed in Nunez et al.[37]). Transfers of carbon, nutrients and water between plant roots and mycorrhizal fungi, first imaged by Nuccio et al. in 2013 [76], are particularly well suited to nanoSIMS analyses, as these exchanges occur across a

microscale interface [76-84]. In soil, nanoSIMS imaging has the potential to measure biogeochemical exchanges between diverse phases, including bacteria, fungi, minerals, organic matter and phages, although the extreme spatial complexity demands a large number of analyses to provide statistically robust conclusions. Since Hermann et al.'s early perspective article[28], many dozens of nanoSIP studies have explored soils, including the fate of isotopically enriched plant amendments to soil[29, 85-88], so-called 'rock-eating' microbes that weather primary minerals[85], the incorporation of microbial necromass into soil organic matter[87], and soil clay minerals that exhibit antibacterial properties[89, 90]. Creative applications, including nanoSIMS analysis of µl quantities of soil porewater[88] and cells separated from the soil matrix via Nycodenz gradients[46, 91] can help to deconvolve the isotope enrichment or elemental stoichiometry of distinct soil pools. Viral and phage particles are a final frontier for nanoSIMS imaging, since their size is at the outer limit of technical feasibility[92-94]. Novel approaches, such as low energy ion implantation (see below), may help to preserve material from such tiny particles, which are so thin that much of the sample is sputtered away in the initial moments of an analysis, when the sputter rate can be 100 times higher than the equilibrium rate [94].

Environmental systems biology studies using nanoSIP have also expanded in breadth in the past decade, and now reach far beyond queries of C and N fixation and elemental distribution. Using imaging of time-resolved isotope tracing studies, Stuart et al., Hong-Hermesdorf, Miethke et al., and Finzi, Pett-Ridge et al. all illustrated that cells can hold resources in temporary storage molecules (respectively—extracellular polymeric substances, acidocalcisomes, cyanophycin) until needed for later use[23, 48, 95-97]. NanoSIMS analyses have also been used to characterize the ecophysiology of novel uncultivated organisms[98, 99], and the cell to cell variability of growth and fixation rates within populations[44, 100-103]. As these studies illustrate, individual cells can have widely different assimilation patterns even within highly clonal and synchronized populations. In recent years, studies of cellular metal uptake and intracellular distribution have proliferated[47, 48, 104] (see also citations in Nunez et al.[37]), in part due to advances in O^- primary beam sources (see below). Many such studies have explored Fe metabolism, and the spatial localization of organisms using Fe as an electron donor or acceptor [105-107].

Multiple innovations have advanced the use of nanoSIP for systems biology applications. These include more accurate isotope assimilation enrichment calculations [41, 108], automated particle analysis software (and thus more highly-replicated studies)[41, 109], and use of various forms of spatial statistics (where phenotypically similar features are grouped based on their nanoSIMS chemical and isotopic fingerprints)[49, 110]. Below, we discuss these and several other notable methodological advances, including a new negative oxygen ion source, low energy ion implantation, improvements in sample preparation and combined imaging and correlated analyses.

Recent nanoSIMS Instrumentation Innovations

The most notable technical advance for nanoSIMS in the past decade was the development of a high-brightness negative oxygen ion source, which enables positive secondary ion imaging with 50 nanometer resolution. In the CAMECA nanoSIMS instruments, imaging resolution is determined by the ion optics, and originally, only the micro Cs^+ ion source had sufficient brightness to achieve a 50 nm spot size; the lower brightness of the duoplasmatron source (used to generate O^- ions) allowed 100 nm resolution at best, with lower stability and reliability. As such, many researchers prioritized Cs^+ analyses for electronegative elements like C and N over O^- analyses for metals.

In 2013, Oregon Physics (Hillsboro, OR, USA) produced a high-brightness O^- source called the *Hyperion II*, which generates ions from oxygen gas using a radiofrequency (RF) inductively coupled plasma (ICP)[111, 112]. The Oregon Physics system substantially suppresses electron extraction while producing a high-brightness O^- beam. Based on tests with Lawrence Livermore National Laboratory's NanoSIMS 50, the Hyperion II was modified to achieve ~50 nanometer spatial resolution, and allow imaging of low micromolar concentrations of metals in biological materials with ~250 nm resolution (**Fig. 4**). Furthermore, the Hyperion II output is very stable (<1% drift over 24 hours) with a low maintenance requirement (every 1 to 3 years). As a result, it is now the preferred O^- source for the CAMECA NanoSIMS 50L[113]. The superior performance of this new source has the potential to attract more researchers to trace metal analysis in biological systems. In our own research, it has enabled higher throughput, as well as spatial resolution sufficient for sub-cellular imaging[47].

Another notable technological advance is the new low energy ion implantation capability for the CAMECA nanoSIMS instruments (extreme low impact energy, or EXLIE) which opens the potential for analysis of smaller and thinner samples. In dynamic SIMS instruments like the NanoSIMS 50, the analysis ion beam controls the yield of desired secondary ions, with a Cs^+ beam used for negative secondary ions, and an O^- ion beam for positive secondary ions. However, this enhancement effect is weak at the sample surface because ions from the analysis beam are implanted some 10s of nanometers below the surface. This is problematic for samples that are only 10s of nanometers thick, such as viruses. To overcome this challenge, Cabin-Flaman et al. demonstrated that initial Cs^0 deposition resulted in a ~10 increase in ion yield at the surface, allowing them to image strands of combed DNA[114, 115]. In response, CAMECA has released a hardware and software package that allows the operator to reduce the analysis beam energy to only a couple hundred volts so that the beam effectively coats the sample locally. In our experience, this system works well, but Cs^+ is incompatible with gold coated samples (presumably the Cs interacts with the gold, not the biological sample). Further use of EXILE should enhance quantitative analysis of extremely other extremely thin particles such as phage and viruses, DNA and RNA, cell membranes and lipid rafts, exudates, and other small and thin biological materials.

Moving toward standardized methods

While nanoSIP has become widely used by the fields of systems biology and microbial ecology, due to the limited number of instruments, the application of high spatial resolution SIMS to biology is still limited to a couple dozen labs and user facilities, each with its own protocols for analysis, standardization and data treatment. A number of important issues are still not codified in the literature and not widely reported in nanoSIMS-based publications:

1. Standards to demonstrate proper operation and tuning of the instrument and for quantification of isotopic ratios and elemental concentrations.
2. Effective mass resolving power (see Section 3.4.1) and demonstration of negligible collection of isobaric interferences
3. Pre-analysis ion implantation and sputtering equilibrium
4. Demonstration of sample performance (charging, flatness, orientation)
5. Data extraction protocols, including defining regions of interest
6. Effects of sample preparation

As the systems biology community continues to elaborate on the nanoSIP approach, it will serve the community to have a more standardized approach. In the methods description that follows,

we describe a series of protocols that could serve as a basis for standardization.

2. Materials

2.1 Sample selection and experimental design

1. Cultures, co-cultures, natural communities from soil, water or sediment, tissues
2. Treatments and controls, harvests from a temporal series (if desired)
3. Final preparation must fit within a 50 mm circle and be vacuum compatible.

2.2 Incubations for stable isotope probing cultures and microbial communities

1. Substrates labeled with stable isotopes. These can be purchased from companies such as Cambridge Isotopes, Isotec-Sigma or JPT Peptide Technologies. Substrates may also be grown (e.g. ^{13}C and ^{15}N plant litter) or purified in house[96].
2. To label cultures with gasses or gas-exchangeable compounds: sealed vials, gas bags, or environmental chambers. For gas injection: gas tight syringe, gas tank regulator, and extraction port.
3. Any inert container can be used for labeling experiments with non-gaseous compounds. Field labeling is also possible if a portion of the system can be at least partially sealed off.

2.3 Sample preparation and pre-analysis characterization

1. While fixation is not always necessary, when used, fixation options include: glutaraldehyde, paramformadehyde, formaldehyde, ethanol, fast freezing, and high pressure freezing.
2. Embedding options; epoxy, acrylic, elemental sulfur, sucrose, OCT, paraffin.
3. Cutting options: Cryostat, ultramicrotome, razor blade, focused ion beam (FIB) [116].
4. Sample support options: Si wafers; Transmission Electron Microscopy (TEM) grid; filter; indium tin oxide (ITO) coated glass slides; vector bond, poly-L-lysine, egg white.
5. Sample mapping options: epi-illumination, phase contrast, fluorescence, electron microscopy.
6. Coordinate encoding; light and electron microscopy systems can be used
7. Conductive coat options: Evaporator or sputter coater with carbon, gold, iridium, or platinum.

2.4 High spatial resolution SIMS

1. The NanoSIMS 50 and NanoSIMS 50L (CAMECA) are state of the art instruments for isotope and elemental imaging. These nanoSIMS instruments are a form of magnetic sector SIMS with high spatial resolution (down to 50 nanometer), high mass resolving power and transmission, and simultaneous detection. They use a high-energy primary ion beam to interrogate the sample (sputtering). In this process, a small volume of the sample is impacted by the primary ion beam, breaking bonds and ejecting atoms and small molecules. A fraction of the sputtered material spontaneously ionizes, in proportion to the element-specific ionization probability. The ions are extracted by an electric field into a secondary ion mass spectrometer. The sensitivity ranges from detecting 1 in 20 nitrogen atoms to 1 in 1,000,000 helium atoms, and mass resolving power (specificity) can be up to 15,000 M/ΔM in corrected units (see Section 3.4.1) [7, 11]. Imaging is achieved by scanning the primary beam over the sample (in a region < 50 μm^2) and reconstructing the ion images digitally.

2. Certified standards can be acquired from the U.S. National Institute of Standards and Technology (NIST) or equivalent agencies, though few are relevant for systems biology

nanoSIP studies. Reference standards can be generated 'in house' by characterizing samples by bulk methods and verifying high resolution homogeneity by replicate SIMS analyses. A further option is ion implantation in epoxy or other surrogate biological materials [117]. Tuning samples can be cell cultures or other materials of known composition (e.g., NBS610 from NIST or a piece of metal) used for instrument tuning and mass selection.

2.5 Data analysis

1. NanoSIMS image analysis software (L'image, L. Nittler, Carnegie Institution of Washington
2. WinImage, Cameca
3. OpenMIMS (https://nano.bwh.harvard.edu/openmims), an add-on for Image J, a free-ware program available from the U.S. National Institutes of Health (http://rsb.info.nih.gov/ij/download.html)
4. Look@NanoSIMS[118], a free-ware program developed for MatLab (MathWorks)

3. Methods

3.1 Sample selection and experimental design

A wide range of biological samples can be analyzed by nanoSIMS if properly prepared (see **3.3**). Experimental effects should be maximized to allow for high spatial resolution analysis: ideally with isotope enrichment >1 atom % or trace element concentration differences that are >2-fold. Typically, treatment samples are referenced to control samples. For nanoSIP experiments, useful controls include no-heavy isotope addition controls (e.g. ^{12}C), and time-zero isotope addition controls. If an isotopically labeled solid substrates has been used as an amendment (e.g., ^{13}C plant material, necromass, EPS[87, 96, 119-121]), it is essential to analyze some of the same material 'neat'—to understand its microscale heterogeneity. For trace element studies, no-treatment controls are likely sufficient. For many experiments, time course analyses aid data interpretation[23, 95, 100-102]. Finally, while nanoSIMS analysis time is frequently costly and limited, biological replicates are essential for each timepoint and treatment and will substantially improve statistical power.

3.2 Isotopic labeling of cultures and microbial communities

If an isotope label is to be tracked, the labeled substrate will depend on the experimental goals, but can range from dinitrogen gas to amino acids to complex biomolecules such as cellulose. Typically, ^{13}C and/or ^{15}N are added as tracers in nanoSIP studies because they can be used without altering cellular function (**Figs. 1, 2**). Other options include $^{18}O_2$ and ^{2}H labeled substrates and water. Elemental labels such as F, Br and I can also be used as tracers [22, 122]. For example bromine-labeled deoxy-uradine (BrdU) may be used as a DNA tag to track cellular division [24, 123, 124], and can be used to track the fate of a Br –labeled nucleic acids (**Fig. 5**). Methods for introducing isotopically labeled substrates can follow the pattern established by stable isotope probing (SIP) [125, 126], a set of widely accepted techniques used in microbial ecology. As a general principle, incubation experiments must last significantly longer than the time of diffusion into the sample, however a balance must be struck in order to avoid cross-feeding effects. Depending upon the research goal, each labeling experiment will necessarily have minor differences, though many may resemble the following example protocol, which was used to ^{13}C and ^{15}N label a freshwater cyanobacteria culture [25] (**Fig. 6)**.

A. oscillarioides was grown in liquid culture with standard conditions, nutrients, buffer and trace element amended media [25]. Exponential phase cultures were transferred to sealed serum vials with no gas phase. Thereafter, a 24 hr incubation occurred with a 12 h light: 12 h dark illumination regime. At the outset of the pulse labeling, 0.07 ml of $NaH^{13}CO_3$ (~99 atm % ^{13}C, 0.047M, final enrichment of 1.7 atm % ^{13}C-dissolved inorganic carbon) and 0.3 ml of 99 atm % $^{15}N_2$, 0.57 mM, final enrichment of 13.6 atm % $^{15}N_2$) were injected into each vial. Basic environmental factors (irradiance, temperature, pH, starting inorganic N and C pools) were measured during the incubation period. At multiple time-points (0 min, 15 min, 30 min, 1 hr, 2 hrs, 4 hrs, 8 hrs, and 24 hrs), a vial was destructively sampled and cells were fixed with 2 % glutaraldehyde in order to determine uptake rates over the diel cycle.

Following a ^{13}C and/or ^{15}N tracer experiment (e.g. with compounds such as ^{13}C-substrate, $^{15}N_2$ or $^{15}NH_4^+$), the rate of C or N assimilation may be quantitatively determined with nanoSIMS data. In general, exposure periods should be kept brief relative to the doubling time of microbial populations, and sub-samples should be harvested at multiple time-points during the isotope incubation in order to measure and minimize recycling and leakage, which for N can approach 35% of newly fixed material [52]. As the nanoSIMS measures total elemental or isotopic signal, and does not discriminate between nitrogen derived from NO_3^-, NH_4^+, or amino pools, measurements yield net uptake only, not gross assimilation. The amount of C or N lost from a cell due to secondary metabolite production, denitrification, leakage, or sample preparation effects cannot be precisely measured with nanoSIMS analysis. If we define assimilation strictly as the uptake of exogenous C or N and its conversion into organic forms, nanoSIMS measurements will bulk all new ^{13}C or ^{15}N taken up regardless of whether the organism has utilized it for organic biosynthesis or not.

3.3 Sample preparation and pre-analysis characterization

Sample preparation is critical to the success of any nanoSIP experiment, and in some cases is the most challenging step. SIMS is an ultra-high vacuum (~10^{-10} Torr) technique, and samples must be prepared for the vacuum chamber in a way that preserves the molecular and elemental distribution of interest. NanoSIMS imaging cannot be used for *in vivo* studies, and samples cannot be analyzed in an aqueous phase without a cryogenic stage[127]. To prepare samples, it is often necessary to stabilize biological components (fixation), remove water (dehydration) and salts (derived from growth media or sea or sediment water), mount samples on a conductive support (Si wafer, TEM grid) and then proceed to either an intact sample analysis, or follow with embedding and sectioning. For some non-aqueous sample types (soils, fungal hyphae), we have found it workable to analyze unfixed samples[28, 87]. For other samples, it is ideal to separate cells or particles from a matrix prior to nanoSIMS analysis; in these cases, a Nycodenz gradient, flow cytometry or microfluics approach can be used [46, 91, 103, 128, 129].

3.3.1 Sample flatness and conductivity

While ideal samples are flat with no more than nm-scale variations in surface topography, in our experience, it is possible to work with non-flat samples. The primary concern topography introduces is increased error in isotopic measurements, which result from spot to spot variations in ion extraction conditions, and effectively detune the mass spectrometer. On a perfectly flat sample (e.g., individual spores), ~1 permil (‰) precision is possible when imaging with electron multipliers. However, with large cells, soil particles or other sources of surface irregularity, only

percent level precision is often possible. For a given sample type, it is necessary to establish the precision of the measurement conditions by using comparable samples to the samples of interest. In most cases, control samples that were not exposed to isotopically labeled substrates are the best option. In many nanoSIP studies, the goal is to achieve isotopic enrichment of 10% or higher (100 permil); at these enrichment levels, even many μm of surface topography can be tolerated[63, 110].

Because SIMS instruments use an ion beam to interrogate the sample and extract ions and electrons, sample charging is a critical consideration. If the sample charges, the extracted secondary ions will have the wrong energy with respect to the tuning of the secondary mass spectrometer, resulting in a loss of mass resolving power and potentially a shift in the mass line. This is primarily an issue for the analysis of negative secondary ions because a significant current of electrons are extracted while a beam of Cs^+ ions are being deposited in the sample. If the sample is nonconductive, the sample will rapidly charge, ruining the analysis. As a practical matter, sample charging can be identified when there are sample regions that appear to have close to zero secondary electron counts. To minimize charging during nanoSIMS analysis, samples (whether intact or sections) are typically coated in an evaporator or sputter coater with a 2 – 20 nm layer of gold or other conductor (e.g. carbon, iridium, and platinum). As a general rule, the more topography the sample has, the thicker the conductive coat needs to be to bridge topographic gaps.

For biological samples in the absence of minerals, sample charging is generally not a problem (even though biological materials are inherently non-conductive). After sputtering equilibrium is reached, the sample becomes sufficiently conducting to perform high quality analyses. For this same reason, analyses can be performed on filters without having to do more than deposit a conducting coat on the surface to enable the charge to dissipate to ground. In fact, monolayers of cells on a conducting substrate can be analyzed (without a conductive coat) because the sample stops charging after sputtering. Nonetheless, at LLNL, we normally apply a conductive coating our samples to facilitate initial imaging.

Samples with a high mineral or salt component often present a greater challenge. Most minerals will charge under Cs^+ analysis after the conductive coat is sputtered away. In these cases, an electron flood gun is needed for charge compensation. While not overly difficult, the electron flood gun does add complexity to the analysis and secondary electron imaging cannot be performed at the same time.

For samples that are to be analyzed intact, some will need to be washed in deionized water to remove salts or other compounds that could coat cells or mineral particles and interfere with ion extraction. For cells or particles, washing on a filter is very efficient, and nucleopore or polycarbonate filters can be used as a sample substrate if they are flat at the micron scale. Other ideal sample substrates include Si wafers, plastic slides, and indium-tin-oxide (ITO) coated glass slides. Conductive sample substrates are preferred to insulators, which will charge as soon as the conductive coat is sputtered away. Cell cultures grown on a solid substrate can be gently washed with repeated immersion in deionized water. Poly-L-lysine, vector bond, egg white or other surface coatings are useful to enhance adhesion to the sample substrate.

3.3.2 Fixation

Fixation of biological tissues is designed to preserve cell morphology and immobilize analytes of interest for imaging analysis. Chemical fixatives (glutaraldehyde, paraformaldehyde, formaldehyde, ethanol, osmium tetroxide [130-132]) work well if proteins and other structural

molecules are the targets. For these analyses, any fixation approach that is suitable for Scanning Electron Microscopy (SEM) imaging will likely work for SIMS imaging. However, more complex methods such as low temperature methods (flash freezing, and high pressure freezing, [133-135]) are sometime warranted to preserve the distribution of small molecules and diffusible ions in biological samples. It is best to avoid applying the stains typically used in EM imaging (e.g. uranyl acetate) in cases where the elemental composition of the sample is of interest. It is also important to recognize that fixatives can cause significant isotope dilution; several nanoSIP studies have shown a stepwise dilution of isotopic composition after chemical fixation, FISH and CARD-FISH protocols [34, 136, 137].

The selection of a fixation procedure is a practical matter—if no fixation is necessary, none should be used. When needed, chemical fixatives can be added directly to samples in solution at concentrations ranging from 2-4%. But the effects of fixatives may be highly sample dependent, and the SIMS community has reported widely differing experiences. Glutaraldehyde is a very aggressive cross-linking agent and is thought to be incompatible with other treatments, such as FISH. Osmium tetroxide is known to cross-link phospholipids. Fixation is not necessary for bacterial spores [26] and potentially encysted microbes. By contrast, vegetative cells are prone to lysis without fixation, especially during washing to remove salts[25]. Herman *et al* [138] report only 35% of photosynthetically fixed ^{13}C was retained as protein in symbiotic algae, following chemical fixation in a glutaraldehyde: paraformaldehyde mixture. In our experience at LLNL, mean nanoSIMS isotope ratios of cyanobacteria fixed with glutaraldehyde correspond well with the isotope enrichment measured in the same cells via IRMS [23, 25], as long as enrichment values are less than 50 atom %.

Cryogenic methods of tissue fixation are presumed to be more conservative, but are substantially more laborious, and flash freezing and high pressure freezing can only be applied to sample aliquots or very small samples [131]. In studies where significant migration of the element of interest is likely to occur during sample preparation, low temperature methods such as freeze-drying may be the best solution [47, 139], but more work is needed to demonstrate quantitative elemental distribution retention.

3.3.3 Embedding and Sectioning

In cases where the goal is to target intercellular elemental or isotopic distribution (e.g. **Figs 1, 2, 3, 7**), embedding and sectioning will likely be needed prior to nanoSIMS analysis. As with other aspect of sample preparation, the embedding and sectioning method should be chosen with the target ions and molecules in mind. Key questions to consider are:

i. Will *in situ* hybridization or antibody labeling be performed on the section?
ii. Are diffusible ions or molecules of interest?
iii. Will the embedding medium be a significant source of interference with the target species?

If none of the above cases apply, then standard embedding methods will likely work and have previously been used to localize ^{13}C- and ^{15}N-labeled structural molecules [23, 24, 27] and fragile marine aggregate [140]. Samples can be embedded in a number of polymers for room temperature sectioning (e.g., epoxy, acrylic, paraffin [134]). Where larger areas need to be analyzed, histological methods can be used [141]. *In situ* hybridization or antibody labeling require the fewest modifications to standard embedding methods for successful labeling. The fixative should minimize cross-linking of the target (e.g. paraformaldehyde instead of glutaraldehyde), and the embedding medium should allow exposure of the target molecules. For resin embedding, acrylic

tends to penetrate samples more readily in our experience. Even better nanoSIMS results can be achieved if the embedding medium is porous or removed after sectioning, such as with most histological and cryogenic methods [134, 141].

If diffusible ion and molecules are of interest, embedding methods that employ room temperature liquids should be avoided. FIB (focused ion beam) sectioning is likely the best option for preserving the distribution of diffusible species because a fully dry sample can be sectioned, however, the method requires specialized equipment and limited sample material can be processed (TEM sections are particularly time consuming to make by FIB sectioning). If the samples are only destined for SIMS analysis, top-cutting may be a more rapid option [116]. One other potential alternative is sulfur embedding [142-144] which we have used to section heterogeneous soil aggregates[28].

A final embedding/sectioning option is cryogenic sectioning, which can be performed with sucrose, OCT or similar compounds. Cryosectioning of water-ice embedded samples is also an option, but is challenging. Cryogenic methods will only preserve the distribution of diffusible ions and molecules if there is no cyro-protectant infiltration and fast freezing is employed; both are major changes from standard protocols and not easily implemented. In particular, removing the cryo-protectant (e.g., sucrose) from these protocols leaves the frozen section brittle and very difficult to section.

Sectioning can be performed with an ultramicrotome, a standard "histological" microtome or cryostat, or even with a razor blade, depending on the type of pre-nanoSIMS imaging that is desired. Standard TEM-grade ultrathin sections (~100 nm) can be analyzed by nanoSIMS, however more data can be collected from thicker sections (up to 500 nm) if lesser TEM image quality is acceptable. Thicker sections are also desirable if large areas (millimeters^2) need to be imaged or analyzed. If transmission light imaging is necessary during the sample mapping phase, indium tin oxide (ITO) coated glass slides are preferable to uncoated glass slides because they do not charge in the SIMS. An adhesive surface coating (e.g. poly-L-lysine) is necessary to retain cryogenic sections during washing or staining. Focused ion beam (FIB) milling can be used as an alternative to embedding and sectioning [116], particularly where the user needs to have precise control over the location and orientation of the section. All thin sections can be laid onto a TEM grid or directly on a solid substrate prior to nanoSIMS analysis.

As an example of a general procedure for sample preparation, before nanoSIMS microanalysis, the filaments of *A. oscillarioides* (described above) were fixed with glutaraldehyde, filtered, washed with Milli-Q (18 MΩ) H_2O, transferred onto a silicon wafer and dried. Since the filaments were sufficiently large, light microscopy was used for navigation and target identification (**Fig. 6**).

3.3.4 Sample mapping

Sample mapping is the final critical step prior to nanoSIMS analyses; it can greatly enhance operator efficiency and is often essential to interpretation of results. Most nanoSIMS instruments have the equivalent of an epi-illumination microscope for sample navigation, and therefore epi-illumination micrographs provide the best reference images for general navigation. SEM mapping (and TEM, or Scanning Transmission Electron Microscopy (STEM) for thin sections) can also positively identify targets for analysis; these images are often comparable (though with higher resolution) to the secondary electron or ion images generated in the nanoSIMS. An ideal series of mapping images should capture the whole sample scale, as well as individual target analysis locations, with reference points that can be used to translate from one image scale to the

next. For target points that are difficult to find in the nanoSIMS light imaging system, such as very small or complex targets, coordinate encoding (relative to obvious fiducial points) can aid navigating for analysis. Matrix-based coordinate transformations simplify the translation of coordinates to the nanoSIMS, which has a somewhat non-intuitive coordinate system. When analyzing samples on Si wafers, we often make faint scratch marks with a diamond-tipped pen before the sample is deposited, this helps to provide unique reference points.

3.4 NanoSIMS analyses

High spatial resolution SIMS (better than 0.5 micron lateral resolution) is necessary to characterize the isotopic and elemental composition of individual microbial cells. The CAMECA NanoSIMS 50 and 50L are the state-of-the-art for combining high lateral resolution, high mass resolution and high transmission, and may be used for both stable isotope and trace element analyses of microbial samples (outlined below). These instruments have two modes of analysis: a Cs^+ primary beam to generate negative secondary ions, or an O^- primary beam to generate positive secondary ions. As a general rule, electronegative elements (e.g., halides) are detected as negative secondary ions, and electropositive elements (e.g., metals) are detected as positive secondary ions. Manufacturer manuals and standard references on SIMS can provide additional guidance on the choice of detection polarity [117]. In some cases, an experiment requires both electronegative and positive elements to be mapped in the same sample. This is possible, but changing polarities is a multiple-hour effort. Alternatively, at high enough concentrations, some elements can be imaged with sufficient sensitivity in their non-typical polarity (e.g., FeO^- instead of Fe^+; C^+ instead of C^-, P^+ instead of P^-; **Fig. 4**) [26, 47, 117].

For any analysis, it is useful to have standard samples that are routinely used for tuning. This allows session to session comparison of transmission, mass resolving power (MRP), and elemental or isotopic ratios. Standards are also important for finding the correct species, which can be particularly challenging for higher masses. Simple reference materials (e.g., iron) are easier to work with than multi-element standards like the National Institute of Science and Technology's NBS610, which has 500 μg/g of most elements. However, there are characteristic spectra for NBS610 that can be used for mass calibration, such as the $^{56}Fe^+$ peak below a ~100x larger $^{40}Ca^{16}O^+ + Si_2^+$ peak at mass 56. Setting up for carbon and nitrogen isotope measurements can easily be done with any biological sample.

3.4.1 NanoSIMS tuning and estimating mass resolving power

Tuning a SIMS instrument requires expert knowledge. The central aspects of SIMS instrument tuning are primary ion beam alignment, peak shape, mass selection and resolving isobaric interferences—all of which are important variables to report on in a nanoSIP article's methods description. Here we present the basics issues.

The alignment and focus of the primary ion beam (analysis beam) sets the location of the ion source for the secondary mass spectrometer and determines the quality of the ion images. Grid samples are typically used to identify and correct for distortion and calibrate the scanning scale. If high current sputtering is used to reduce the time to achieve sputtering equilibrium, the higher and lower current beams need to be aligned. This alignment should be done before finalizing the tuning of the instrument because sometimes it is better to move the lower current beam position toward the higher current one to optimize ion current or quality of the focus.

To obtain accurate measurements, the instrument must be tuned and aligned to collect the ions of a species of interest to the exclusion of other species at the same nominal mass. The

secondary ion beam for the species of interest must be tightly focused at the detectors and multiple beam diameters from adjacent masses, and the detector must be aligned to collect effectively 100% of the transmitted ions of interest and only those ions, with room for small variations in the magnetic field or other potential shifts in the mass line. The result is a peak that is flat-topped and steep-sided. A metric of the peak shape is the mass resolving power (MRP), which is also a metric of the ability to resolve adjacent masses. MRP is defined based on the nominal mass, M, at which the measurement is made, and the resolvable difference in mass, ΔM, between two adjacent species:

$$MRP = M/\Delta M. \quad (1)$$

Because of the proportional nature of this metric, the measured MRP of the mass spectrometer is effectively applicable across all masses. It is important to note, however, that the resolvable difference in mass increases with mass. The CAMECA NanoSIMS software uses the steepness of the side slopes of the mass peaks as a measure of the mass resolving power of the secondary mass spectrometer.

$$MRP \cong R/(4 \cdot L90), \quad (2)$$

where R is the effective radial distance of the detector position and L90 is the average lateral distance between the 10 and 90% height of the peak side slope. This estimate of mass resolving power is ~1.5 times higher than the effective MRP based on the standard definition of MRP, and in our publications, we report the MRP of our analyses based on this correction (**Fig. 8)**. Regardless of the MRP value reported, it is essential to be aware of all potential interferences and ensure that their contribution to the measured mass line is negligible. Simply observing that a peak top looks flat on a standard is not sufficient to be sure there is not a significant unresolved interference. Blanks and control samples are important for checking for interferences, as are software programs that can calculate potential interferences.

Peak shape is an integrated function of everything from the primary beam location and size to the gain on the detector. A tightly focused primary beam reduces the abundance of off-axis ions, which cause angular aberration. A well centered primary beam relative to the secondary ion collection lenses minimizes potential distortion. The secondary ion beam should be aligned relative to all the lenses, slits and apertures in the secondary mass spectrometer to maximize transmission and minimize distortion. The entrance slit width is selected based on the target MRP, an aperture slit (similar to a field aperture for the CAMECA ims series) is used to reduce angular aberration, and an energy slit is used to reduce chromatic aberration, along with other tuning. The detector gain and threshold must be set to exclude noise and register >90% of the incident ions. In our experience, dimers (e.g. $^{12}C^{12}C$, or $^{12}C^{13}C$) result in higher gain than monomers, and the detector voltages must be adjusted accordingly. Incorrect detector settings or a failing detector can result in sloped peak tops. It is also important to set detector deflector settings so that the ions strike a region of the detector first dynode with a flat response to scanning, to achieve a flat top peak. Finally, for a NanoSIMS 50 or 50L, it is important to keep sustained count rates below ~300,000 counts per second to prevent premature aging of the electron multipliers. Sustained high count rates can result in dead spots on the detector first dynode and overall loss of sensitivity from carbon deposition on the other dynodes.

3.4.2 Cs^+ analysis for electronegative elements and isotope ratios

The vast majority of system biology studies requiring nanoSIMS analysis are focused on electronegative elements such as H, C, O, N, P and S [39]. All of these elements (and their corresponding isotopes) are analyzed with a Cs^+ primary beam. Of these, combined C and N

isotope measurements are the most common and stringent analyses at the low end of the periodic table; we discuss their analysis in detail below.

For both of carbon-13 and nitrogen-15, the higher sensitivity is achieved using a Cs^+ primary beam and extracting negative secondary ions. The rare and major isotopes are both mapped in the sample, and the ratio of the two reveals the distribution of the incorporated label in the sample (**Fig. 1, 2, 6, 9**). Nitrogen is typically detected as the molecular ion CN^- because of the poor yield of N^- and N^+ [145, 146]. Carbon isotopes can be measured using the monomers (C^-), the hydrides (CH^-), the dimers (C_2^-), or the CN species (where mass resolving power requirements increase respectively). The CN species typically have the highest ion count rate in biological samples, but because ~12,000 MRP (~18,000 based on the CAMECA software) is required to resolve $^{13}C^{14}N^-$ from $^{11}B^{16}O^-$ at mass 27, these species are typically only used when the highest surface sensitivity is required[147].

We have found that the C_2^- dimers measured at mass 24 and 25 are more compatible with the CN^- species (e.g., $^{12}C_2^-$, $^{13}C^{12}C^-$, $^{12}C^{14}N^-$, $^{12}C^{15}N^-$) because of similar secondary ion focusing (**Fig. 10**). Simply put, the maximum transmission for the carbon dimers is better aligned with the maximum transmission for CN^- than the carbon monomers are. Physically, this means that the optimal focusing voltage for the lens used to focus the secondary ion beam in the entrance slit to the mass spectrometer is more similar for C_2^- and CN^- than for C^- and CN^-. Because the ions are all detected simultaneously, only a single E0S focusing voltage can be used, and therefore if C^- and CN^- are measured, the E0S focusing voltage has to be compromised for one or both sets of species. This compromise not only results in a loss in transmission, but it also very likely results in lower reproducibility of isotope ratio measurements. Maintaining optimal focus at the entrance slit is important to isotope ratio measurement reproducibility. The difference in the difference in E0S focusing voltage for these species is likely due to the differences in energy spectra resulting from C_2^- and CN^- primarily coming from molecule decomposition during flight, while C^- is generated at the sample[148]. We have observed that the offset between C^- and CN^- varies, but we have not succeeded in making this offset acceptably small. We have also observed that there is often a measurable offset between C_2^- and CN^-, but it has always been relatively small (<10 V; **Fig. 10**).

The $^{15}N/^{14}N$ ratio can be directly calculated from the ratio of the CN ions ($^{12}C^{15}N^-/^{12}C^{14}N^-$). The $^{13}C/^{12}C$ ratio, however, equals $^{12}C^{13}C^-/(2 \times {}^{12}C_2^-)$ based on:

$$\left(\sum_{i=12}^{13}\left[{}^{i}C\right]\right)^2 = \left[{}^{12}C\right]^2 + \left[{}^{13}C\right]^2 + 2\left[{}^{12}C\right]\left[{}^{13}C\right], \quad (3)$$

where $[^iC]$, the relative abundance of the respective isotopes, and the individual terms on the right hand side of the equation are the expected relative abundances for the respective combinations of species [149].

Typical analytical conditions for nanoSIMS are: a ~2 pA Cs^+ primary beam focused to a nominal spot size of ~100 nm, a 256 x 256 pixel raster over a 10 x 10 micron^2 area, a dwell time of 1 ms/pixel, the secondary mass spectrometer tuned for five to seven secondary ions (e.g., $^{12}C_2^-$, $^{13}C^{12}C^-$, $^{12}C^{14}N^-$, $^{12}C^{15}N^-$ and $^{31}P^-$) detected on electron multipliers in simultaneous collection mode, ~6500 MRP (~10,000 MRP based on the CAMECA software; see above) to resolve isobaric interferences (e.g. $^{13}C^{12}C^-$ vs. $^{12}C^1H^-$ at mass 25; $^{13}C_2^-$ vs. $^{12}C^{14}N^-$ at mass 26; **Fig. 8**; $^{11}B^{16}O^-$ vs. $^{12}C^{15}N^-$ at mass 27), and data collection for 10 to 20 serial quantitative secondary ion images (*i.e*. layers). For larger areas, the analysis time must be increased proportional to the area. Hundreds of cells may need to be analyzed in order to account for natural variability in metabolism from one cell to another (**Fig. 11, 12**).

When possible, biological samples should be sputtered to a depth of~60 nm before data collection to achieve sputtering equilibrium. The depth of analysis during a measurement is typically between 50 and 200 nm, however whole cells may be consumed to acquire sufficient counts for high precision analyses, to average over the entire cell, or to generate a cell depth profile (**Fig. 13**). The sputter rate for biological materials with a Cs^+ primary beam (16 kV, normal incidence) is 1-2 $nm \cdot \mu m^2 \cdot pA^{-1} \cdot s^{-1}$ at equilibrium [94, 150]. With a 2 pA Cs^+ analysis beam and a 1x1 μm^2 raster, a 1 μm cell can be consumed in a few minutes.

In addition to C and N, the distribution of electronegative elements (e.g., H, O, S and P) or highly abundant electropositive elements (e.g., Fe as FeO^-) can be imaged during stable isotope analyses[87]. These can also include labeling elements such as F, I or Au (*see* Section **3.6**, '*immuno-labeling*')[22, 122]. In some cases, magnetic peak switching may be necessary to image the distribution of all elements of interest; at LLNL we have successfully analyzed up to 20 elements in a single analysis of bacterial spores. Samples can be imaged simultaneously by secondary electrons with negative secondary ions.

3.4.3 NanoSIMS trace element analysis

Trace element analysis in biological samples is often used to determine the concentration and distribution of metal cofactors and labels. With the invention of the Hyperion II RF inductively coupled plasma ion source, trace metal analysis with nanoSIMS has become significantly easier and more attractive. The method of analysis is similar to the stable isotope analysis method outlined above, except that typically the trace elements of interest are metals, which are imaged with higher sensitivity as positive secondary ions with an O^- primary beam [117]; elements such as Na, K, Al, Mg and Ca ionize extremely well in this mode. To determine whether metals such as Mn, Fe, Cu, Mo, Cr, V and Ni (and in the right circumstances, Zn and As) can be detected in a given system with subcellular resolution depends on their concentration in the sample and relative sensitivity factor (a.k.a., relative useful yield; see **3.5.2** and [117]). At LLNL, we have imaged a range of trace elements in cells, including Mo (as a proxy for nitrogenase; **Fig. 11**), Mg, Si, P, Mn, Fe, Cu, Zn and As [47, 48, 104, 151]. The highest spatial resolution achieved with the Hyperion II on a CAMECA NanoSIMS in this mode is ~50 nm with ~0.5 pA O^- primary beam [47, 113]. For very low concentrations elements (ppb to low ppm), a >100 pA primary beam is necessary to acquire enough counts for imaging, with spatial resolution >250 nm (**Fig. 4**). The sputter rate for biological materials with an O^- primary beam is ~0.2 $nm \cdot \mu m^2 \cdot pA^{-1} \cdot s^{-1}$ [150]. For many metals, low ppm-level cellular concentrations can be imaged, but great care must be taken to ensure detectors only collect the isotope or element of interest, as opposed to isobaric interferences.

3.4.4 Standards and controls.

Standards and controls have distinct but related roles that are important to obtaining reliable results. Standards are used to check instrument operation, quantify absolute composition, and provide a reference for other experiments. For high precision isotope measurements or trace element measurements, at least two matrix-matched standards with distinct known compositions are necessary to insure accurate and meaningful results [47, 152]. Experimental controls are used to test for experimental artifacts and the statistical significance of treatments.

Standards are not readily available for biological SIMS because certified biological samples are not appropriate. As a result, standards typically need to be produced and characterized 'in-house' or borrowed from other laboratories. In cases of large effects relative to

analytical uncertainty, no-isotope experimental controls can sometimes take the place of standards. For elemental analyses, it is necessary for the measured ratios of interest to be on the order of 10x higher than background to be confident the effects are real [48, 139] Furthermore, correct instrument operation is hard to verify. One stop-gap option is to always analyze the same sample at every session, even if the absolute composition is uncertain or it is not relevant to the biological sample (e.g., NBS610) [48, 139].

For C and N isotopic measurements, we at LLNL originally used a well-characterized *Bacillus subtilis* spore preparation as a reference standard for [23]. Measurement precision, $\sigma_{(internal)}$ for this standard is 0.4-1.4 % (2σ for individual $^{13}C/^{12}C$ and $^{15}N/^{15}N$ measurements), and replicate analyses yielded an analytical precision, $\sigma_{(std)}$, of 2.1 % (2σ for an individual measurement) (**Fig. 8**). More recently, we use an in-house characterized culture of *Pseudomonas stutzeri* deposited on a Si wafer because these cells provide a better matrix match for our typical experiments.

For high spatial resolution elemental analyses of biological samples, absolute concentration standards are more difficult to establish for multiple reasons. First, concentrations are typically low and therefore prone to contamination. Second, elemental concentrations can vary spatially, making it difficult to relate high resolution analyses with bulk composition. Third, the composition of the elemental concentration standards needs to closely match the unknowns. Beyond these constraints, it is ideal to have multiple concentrations in the relevant range to establish a calibration curve to control for potential isobaric interferences.

The combination of achieving sample homogeneity and matching the composition of the unknown is typically the hardest problem. Concentration standards should be compositionally equivalent to the unknowns because matrix and composition effects are well known to affect relative ion yields [117, 153-155]. Recently Ackerman et al. used homogenized fish tissue mixed with dilute copper solutions to make multiple concentration standards (**Fig. 4**) [47]. Repeated analyses of the material correlated well with bulk concentration data.

In case where biological standards are not available, the NIST glass standard NBS610 is useful for mass alignment of metallic elements and for detector gain control, but not quantification in biological samples. NIST also produces trace element standards for biological materials, but these are large, heterogeneous particle samples designed for bulk analysis and are challenging for SIMS. Reference samples normally have to be made and characterized by the interested lab. A good but expensive alternative for elemental quantification is to have the element of interest implanted in epoxy or another surrogate biological material. The ion implant is then analyzed by depth profiling and integrating over the ions collected from the implanted species [117].

3.5 Data processing and image analysis

NanoSIMS researchers have developed multiple programs that allow nanoSIMS ion images to be displayed and processed to extract the quantitative data (see **2.5**). Data processing should include corrections for detector dead-time and image shift and should enable regions of interest (ROIs) to be defined. The isotopic composition for each ROI is calculated by averaging over all of the replicate scans. ROI definition algorithms can be used to identify cells, partition images into uniform subregions, or define threshold cutoffs for extracting data automatically. Notably, Arandia-Gorostidi et al. and Dekas et al. both used auto-identification to select many 100s of putative cells in their analyses[41, 109], far more than in many early nanoSIMS studies.

3.5.1 Quantifying and reporting isotopic data

As discussed in section **3.4.4**, standards are a critical part of ensuring good instrument performance and accurate data. For isotopic ratios, standards should be used to calculate instrumental mass fractionation (IMF), which can be expressed as:

$$IMF = \frac{R_{STD-meas}}{R_{STD-true}}, \quad (4)$$

where $R_{STD-meas}$ and $R_{STD-true}$ are the measured and true isotopic ratios for the standard, respectively. There is cause for concern if the IMF differs from 1 by more than a few percent. Considering the precision of nanoSIMS (>0.1%), the true isotopic ratio in the unknown, $R_{UNK-est}$, can be estimated from the ratio measured for the unknown, $R_{UNK-meas}$ and the IMF using a gain correction:

$$R_{UNK-est} = \frac{R_{UNK-meas}}{IMF}. \quad (5)$$

The resulting isotopic data can be presented as ratios, delta values, and atom percent excess (APE) (e.g. **Fig. 6**). For tracer experiments, APE provides the clearest indication of the uptake of a stable isotope tracer. APE is calculated based on the initial isotopic ratio of the sample (or organism) at T = 0 (R_i) and the final isotopic ratio in the sample, R_f, [23]:

$$APE = \left[\frac{R_f}{R_f+1} - \frac{R_i}{R_i+1}\right] \cdot 100\%, \quad (6)$$

Note that R is the ratio of the rare isotope to the abundant isotope (e.g., $^{13}C/^{12}C$) and that $R/(R+1)$ is the fraction, f, of the rare isotope of element X, which can be written f_X.

Data can also be presented as net incorporation of the labeled element in the substrate if its isotopic composition and amount are well constrained and it is uniformly available to the sampled organisms. In Popa et al, we defined the term Fx_{net} as the net incorporation of an element (e.g., net carbon incorporation is "F_{Cnet}") [25]. Assuming a two-isotope system, we derived Fx_{net} based on a two-component mixing model that accounts for the minor (Eq. 7) and major isotopes (Eq. 8) of element X incorporated from the initial biomass and the spiked pool:

$$f_{x_f} = F_i \cdot f_{x_i} + F_s \cdot f_{x_s} \quad \& \quad (7)$$

$$[1 - f_{x_f}] = F_i \cdot [1 - f_{x_i}] + F_s \cdot [1 - f_{x_s}], \quad (8)$$

where F_i is the fraction of the labeled element that was initially in the sampled organism and F_s is the fraction of the labeled element that was taken up from the spiked pool. In Popa et al., we originally derived Fx_{net} as a function of initial biomass, solving equations 7 and 8 for F_s/F_i,, yielding

$$Fx_{net} = \frac{F_s}{F_i} = \frac{R_f(1-f_{x_i}) - f_{x_i}}{f_{x_s} - R_f(1-f_{x_s})}, \quad (9)$$

where R_s is the isotopic ratio in the spiked pool, [25]. Here we suggest both a correction and a change to that original equation. The correction is that here we restore the "1–" in the last term of the denominator, which was accidentally omitted in the Popa et al. article. The change is that here Fx_{net} is expressed as a fraction, as opposed to a percentage. While technically this equation applies only to the labeled element, it can be used to estimate change in biomass assuming no change in stoichiometry. We note that it is not necessary to quantify the actual biomass to use this equation.

Unfortunately, defining net incorporation as a function of initial biomass tends to cause confusion because Fx_{net} exceeds 1 (i.e., 100%) after biomass doubles. Therefore to avoid

confusion, we defined a new parameter, X_{net}, which is net incorporation of an element as a function of total final biomass[41]:

$$X_{net} = \frac{F_s}{F_s + F_i} = \frac{F_{x_{net}}}{F_{x_{net}} + 1} \quad (10)$$

Using this formulation, net incorporation of carbon is notated as C_{net}.

3.5.2 Quantifying and reporting elemental data

For biological samples, relative and absolute elemental concentrations are typically determined based on the relative ion count rates for the element of interest, X, compared to a uniformly distributed major element—typically C in most biological samples. This approach may not be valid if the element of interest is in a structure that is low in C relative to the average matrix concentration (e.g. if metal is sequestered in a vacuole). In rare cases, implantation of a reference ion has been used to enable direct quantification in biological samples[156]. To the extent SIMS is used to quantify trace elements in biological samples, researchers tend to use matrix-matched elemental standards.

If a matrix-matched standard for element X is available, the concentrations of element X, $[X]_{UNK}$, can readily be determined based on proportionality using a parameter known as the relative useful yield (*RUY*)[157]. This approach works because SIMS typically yields a linear change in relative ion count rates as the concentration of that species increases in the sample. Ideally linearity is demonstrated in the relevant range using a set of standards. Resolving isobaric interferences is an important aspect of getting a reliable, linear response. The ion yield for the element of interest is normalized to a reference ion. The *RUY* is defined as ratio of the concentrations of element X and the reference element—here C—to the corresponding ion ratio measured for a standard:

$$RUY_{X:C} = \frac{[X]_{STD}}{[C]_{STD}} \cdot \left(\frac{X^+}{C^+}\right)^{-1}_{STD} \quad (11)$$

where $[X]_{STD}$ and $[C]_{STD}$ are the concentrations in the standard of element X and carbon, respectively, and $\left(\frac{X^+}{C^+}\right)_{STD}$ is the measured ion ratio, here shown as positive ions. Note that the concentrations can be in any units, and the ion ratio can be for the measured species (e.g., $^{56}Fe^+$ and $^{12}C^+$) or it can be corrected for the isotope abundances, as long as these choices and the measured species are consistent for the standard and the unknowns. The *RUY* is then used to calculate the concentration of element X in the unknown using:

$$[X]_{UNK} = \left(\frac{X^+}{C^+}\right)_{UNK} \cdot [C]_{UNK} \cdot RUY \quad (12)$$

Note that ideally $[C]_{UNK} = [C]_{STD}$, or else $[C]_{UNK}$ needs to be determined by an independent method. In some work, the *RUY* is define as the inverse, with the appropriate change in Eq. 12.

Relative sensitivity factor (RSF) is a related parameter used in the semiconductor industry[117] that is generally not applicable as defined, but which can be used to estimate the *RUY*.

$$RUY_{X:ref} \approx \frac{RSF_x}{RSF_{ref}} \quad (13)$$

where RSF_x and RSF_{ref} are for the element of interest, X, and the reference ion, which was C above. We have used this approach obtained reasonable estimates of copper in *Chlamydomonas reinhardtii* cells using calcium as the reference ion [48].

In the absence of a standard for absolute quantification, elemental data are typically reported as ion ratios, which is indicated by maintaining the charge symbol (e.g., $^{63}Cu^{+}/^{12}C^{+}$). The mass superscripts are removed if the ratio is corrected for isotopic abundances.

3.5.3 Measurement precision

Measurement precision should be determined based on replicate measurements of the ratio of interest during the analysis by calculating the standard error of the mean (SE). This statistic can be compared to Poisson statistics error for a ratio, σ_{ratio}, calculated from Gaussian error propagation:

$$\sigma_{ratio} = R \cdot \left[\left(\frac{X_{numerator}^{0.5}}{X_{numerator}} \right)^2 + \left(\frac{X_{denominator}^{0.5}}{X_{denominator}} \right)^2 \right]^{0.5} \quad (14)$$

where R is the calculated ratio and X is the number of ion counts for the numerator and denominator, respectively, which would typically be the minor and major isotopes, respectively. Because this calculation is based on a sum of squares, the error for the minor isotope will dominate σ_{ratio} if $X_{minor} << X_{major}$ (e.g., ^{13}C vs. ^{12}C) and σ_{ratio} can be estimated directly from X_{minor} and R:

$$\sigma_{ratio} \approx R \cdot \left(\frac{X_{minor}^{0.5}}{X_{minor}} \right) \quad (15)$$

σ_{ratio} should be compared to the standard error (SE) for replicate measurements of the ratio in the sample. If the measured SE is significantly worse (>2 σ), then there is potential for improving the precision of the measurement based on tuning, sample flatness, or other factors. In practice, the precision of isotope ratio measurements by ion counting is no better than ~1 permil under the best conditions.

In addition to considering these factors, measurement reproducibility from sample to sample and even from subregion to subregions within an image has to be included in the measurement precision when two measurements are being compared, even within the same image. For example, two cells within an image can only be considered statistically different if the difference between the two measurements is greater than the variability of measurements on comparable samples. The potential exists for measured isotopic ratios to vary across a nanoSIMS image for an isotopically homogeneous sample because of sample and tuning problems. This error can formally be incorporated into the measurement precision, by summing measurement error and the location to location variability in quadrature:

$$SE = [SE_{meas}^2 + SD_{tests}^2]^{1/2} \quad (16)$$

where SD_{tests} is the standard deviation of test measurements for location to location variability. The summed errors must be expressed in fractional units, such as permil. While this calculation is simple, ensuring that all the sources of potential error are included is not, and care should be taken when making inferences from small differences in ratios, or large differences with large but seemingly statistically significant precision estimates.

The error discussed so far is internal error, meaning that it only accounts for the variability of a particular set of measurements. For comparison to other measurements and absolute values, external measurement error is estimated from standard measurements using the sum in quadrature approach used above. Because of the potential for shifts in measured isotopic

ratios relative to an absolute value (i.e., IMF) for slightly different samples, caution must also be exercised when using the external error estimates. With all of these issues to consider, researchers typically focus on achieving large relative isotopic enrichments in nanoSIP measurements.

3.6 Combination with synergistic techniques

Coupling nanoSIMS with other imaging or bulk characterization methodologies provides an enormous opportunity to extend inferences and understanding of a sample[158]. By combining nanoSIMS analysis with approaches such as FISH, SEM, TEM, X-ray microscopy, or immuno-methodologies, systems biologists can also explore the physiology of known and uncultured microorganisms by simultaneously collecting functional, phylogenetic, and molecular information from individual cells or particles. While the list of synergistic approaches discussed here is by no means exhaustive, the following technologies have been used in combination with nanoSIMS:

1. "Bulk analysis" (IRMS and ICP-MS): For many studies, it is very useful to initially analyze a bulk sample mass by isotope ratio mass spectrometry (IRMS) to ensure that some isotopic enrichment occurred, and to determine average APE and net-fixation values. To perform isotopic bulk analysis IRMS with small samples garnered from cultures or environmental samples, samples may be filtered onto pre-combusted glass fiber (GF/F) filters, dried, and then analyzed. In our experience, absolute isotope enrichment values of a cell concentrate measured via IRMS can differ significantly from the nanoSIMS analyses because of cell to cell variability and surface contamination; close attention is necessary make quantitative comparisons [137]. Similarly if, trace metal distribution is of interest, it is important to constrain the likely concentrations in individual cells or particles by first analyzing an extract of whole cells or target molecules by inductively coupled plasma mass spectrometry (ICP-MS) [151].
2. Light microscopy: Light images can be useful for navigation in the nanoSIMS CCD view, which also uses light microscopy. Images should be collected at multiple levels of magnification to identify analysis targets and aid in locating them. Post-analysis imaging can be used to confirm targets.
3. SEM: SEM imaging is a relatively fast screening tool and allows pre-identification of particles of appropriate size and morphology with higher resolution than light microscopy (e.g., hyphal and bacterial surfaces; filamentous vs. single cells, amorphous vs. crystalline minerals). SEM images are also frequently useful to guide both pre- and post-SIMS analysis, after regions with unique isotopic or molecular signatures have been identified. If necessary, SEM-EDS mapping can additionally be used to identify basic elemental distribution. Low voltage imaging (<5kV) typically provides better surface characterization of biological or soil samples. SEM can be very useful for guiding and confirming analysis of small or complex targets. SEM images are readily correlated to SIMS secondary electron images, although harder to correlate to nanoSIMS CCD images.
4. TEM, STEM and analytical TEM [23, 48, 63, 159, 160]: EM imaging is useful for identifying ultrastructure in thin and FIB sections, but correlation with nanoSIMS is more challenging than for light microscopy or SEM. Light micrographs are typically needed to help find desired location on transmission electron micrographs.
5. Atomic force microscopy (AFM)[94, 161]: While it has only rarely been used in combination with SIMS, AFM imaging provides nanometer-scale topographic information and can be

performed in liquid under controlled conditions. A group in Luxemburg took the step to incorporate an AFM into a NanoSIMS 50 to allow correlated height measurements without exposing the sample to vacuum [162].

6. FISH, El-FISH and BONCAT: In 2008, several research groups independently developed new approaches which combined nanoSIMS analysis with *in situ* hybridization(EL-FISH [22], SIMSISH [122], and HISH [20]); in each, a phylogentic probe is linked to a highly electronegative elemental label (fluorine, iodine, gold, selenium, or bromine) instead of the typical fluorophore. These approaches enable simultaneous localization of the tag via Fluorescence in situ hybridization (FISH) [163, 164] or Catalyzed Reporter Deposition-Fluorescence In Situ Hybridization (CARD-FISH) [165] and chemical mapping in the nanoSIMS. These approaches can help overcome problems with background autofluorescence in FISH images, because nanoSIMS is used to detect the elemental tag linked to the oligonucleotide probe. The key to this approach is to use highly electronegative elements, such as halides, sulfur, selenium, tellurium and noble metals, which can be detected with very high sensitivity (1 in 20 atoms) in concert with carbon and nitrogen isotopes (for functional characterization). When choosing which elemental tag to apply, care should be taken to ensure the natural background of these elements in low in the sample (e.g. marine sample often have high F background). To date, introducing multiple probes simultaneously (with multiple elemental tags) has proven difficult. It is often possible to simply correlate fluorescent featured in FISH/CARD-FISH images with the isotope ratios of the same locations in nanoSIMS images[34, 41, 54, 75, 137, 166]. It may be possible to use FISH-SIMS approaches in embedded samples; the work of Lemaire et al [167], where fixed samples were embedded in TissueTek® and then cryosectioned and FISH labeled, suggests this may be possible. We caution however, that the application of CARD-FISH may also reduce original cell enrichment by 60-80% for ^{13}C and 30-60% for ^{15}N[34, 136, 137]. Other molecular tagging methods (e.g. BONCAT) may also be combined with nanoSIP studies, particularly for targeting active cells[92, 168].
7. Synchrotron imaging (e.g. STXM and NEXAFS) [87, 169-171]: Spectroscopic techniques allow precise, quantitative measurement of molecular and isotopic patterns in an undisturbed sample, at high resolution, and may be particularly useful for imaging of microbial populations in mineral matrices such as soils and sediments. Scanning Transmission X-ray Microscopy (STXM) can map organic C distribution, image associations of organics with specific mineral types, and has been used to trace organic matter of differing origins into the soil matrix [172, 173]. Research at LLNL shows that nanoSIMS and STXM are quite synergistic, have similar resolution, and together yield data on both molecular class and elemental quantity; STXM data is based on transmission (integrates total volume under the beam), while nanoSIMS can characterize either surfaces or a 3-D volume depending on the method of preparation and analysis conditions. NanoSIMS may be preceded by synchrotron-based x-ray imaging techniques such as Scanning Transmission X-ray Microscopy (STXM) and Near Edge X-ray Absorption Fine Structure (NEXAFS) to determine mineral oxidation state or dominant organic constituents. Sample specimens can be mounted on silicon nitride (Si_3N_4) windows or standard TEM grids without a chemical adhesive. Samples should be analyzed by STXM, then coated with a thin conductive layer of gold or iridium and imaged by SEM, and then by nanoSIMS.
8. Molecular and structural imaging (e.g. MALDI, Raman, TOF-SIMS, X-ray tomography)[91, 174, 175]: Multiple imaging techniques now have the capability to map a molecular landscape with subcellular resolution[158]. While the majority of these approaches do not have the spatial

resolution of NanoSIMS, the sample preparation requirements are similar enough that a single preparation can often be imaged first for molecular distribution, and later by nanoSIMS for elemental or isotope distribution.

9. Antibody labeling or "immuno-labeling" [176, 177]: Antibody-labeled immuno-gold tags can also be used to target the locale of specific proteins within a cell [131, 178]. Initial mapping may be performed by TEM (**Fig. 7**) or SEM with a back scatter detector [179] before nanoSIMS analysis for validation and higher resolution sample mapping.
10. Microarrays (Chip-SIP)[1, 79, 147, 180-182]: Microarrays, while less commonly used than a decade ago, are very compatible with nanoSIP studies and a creative means to measure the isotope ratios of individual biomolecules (RNA, DNA, peptides, proteins, sugars, lectins, etc). They are typically printed with microscopic spots of a biomolecule tethered to a surface (often a glass slide). Our group uses Chip-SIP[1], a technique where community RNA (extracted following an isotope tracing experiment) is hybridized to an ITO-coated slide surface derivatized with either functionalized alkylphosphonates and/or organosilanes and printed with custom 16S rRNA probes[147]. Then, a nanoSIMS is used to quantify the amount and isotope enrichment in the hybridized RNA. Many 1000s of probes can be analyzed in a single nanoSIMS session, and like all nanoSIP studies, Chip-SIP is compatible with dual-label (i.e. ^{13}C *and* ^{15}N) experiments—unlike the traditional SIP method. Because of the unpredictability of probe binding, it is best to design a suite of probes for each taxon of interest. ITO slides and Si slides can also serve as a substrate for DNA deposited and hybridized, or combed DNA, as descried by Cabin-Flaman et al. via 'combing-imaging by SIMS' (CIS)[114, 115].

4. Future Directions

Continued development of the NanoSIMS and related technologies, such as sample preparation and data processing, can broadly benefit systems biology research, and expand the potential for nanoSIP studies. The success of the CAMECA NanoSIMS 50 and 50L has resulted in a steady growth in the number of instruments worldwide, and most scientists with an interesting nanoSIP research problem and some funding can likely gain access to a nanoSIMS through a user proposal, a collaboration, or a fee-for-service arrangement. Other large- and small-geometry SIMS instruments can also be made to work for biological applications (e.g. 7f with hyperion; LG-SIMS; TOF-SIMS). Looking forward, SIMS instrumentation is also continuing to evolve, such as MS-MS ToF-SIMS[162] and FT-ICR SIMS[183], and there are new capabilities for nanoSIMS in development that will lead to higher spatial resolution and instrument sensitivity: in-situ atomic force microscopy (AFM)[162], brighter reactive ion sources[184], a cryogenic stage[127], and the extreme low implantation energy approach discussed above. These advances will particularly benefit those looking to analyze ever-smaller particles (e.g., viruses, DNA), and do quantitative elemental analysis where cryo-preservation is ideal (e.g., subcellular trace metals).

Advances in the technologies that support the NanoSIMS can also make a big difference in the quality and throughput of nanoSIP experiments. More studies with multi-isotope simultaneous labeling can help to distinguish overlaps in metabolism and activity (e.g., heterotrophs, autotrophs, mixotrophs[41]), and differential elemental stoichiometry[46]. Sample preparation is a perennial challenge and any new methods that make it easier to prepare high quality samples for nanoSIMS analysis would advance the field. On the output end, data processing can be time consuming, and improved software and automation would be beneficial

as researchers seek larger data sets. Finally, standardization continues to be an area that needs more effort, but the wide breadth of need and challenges of production are serious hurdles.

The nanoSIP method we describe here is a highly flexible and adaptable approach, enabling the study of isotope and element exchanges and transformations at single cell and sub-cellular level. In microbial assemblages, it can enable identity and function to be directly related to community structure, microgradients, and substrates, and has broad relevance for microbiome studies, both in nature and in laboratory, human, or industrial settings. Researchers using nanoSIP and nanoSIMS can answer basic but previously inaccessible questions about where organisms are within a community and what they are doing there. In many cases, these advances in our scientific understanding require coordinated use of multiple approaches, including sequencing and synergistic visualization techniques. After two decades of application, it is a fully standard method in systems biology, microbial ecology, soils and plant research and cell biology. Researchers have seen the value of this approach and are making the necessary efforts to design experiments and supporting analyses to take advantage of its insights into biological function.

Acknowledgements

We thank Ian Hutcheon, for his many years of mentorship, advice, and leadership of the LLNL SIMS group. We also thank our many colleagues and collaborators, with special thanks to Steve Blazewicz, Anne Dekas, Ben Jacobsen, Xavier Mayali, Erin Nuccio, Rhona Stuart, and Dagmar Woebken. Christina Ramon plays a critical role in helping to prepare and organize many of the samples we have discussed. This work was funded in part by multiple awards from the DOE OBER Genomic Science program and LLNL Laboratory Directed Research and Development program and performed under the auspices of the U.S. Department of Energy at Lawrence Livermore National Laboratory under Contract DE-AC52-07NA27344.

References

1. Mayali, X., P.K. Weber, E.L. Brodie, S. Mabery, P.D. Hoeprich and J. Pett-Ridge, *High-throughput isotopic analysis of RNA microarrays to quantify microbial resource use.* ISME J, 2012. **6**(6): p. 1210-1221.
2. Adamczyk, J., M. Hesselsoe, N. Iversen, M. Horn, A. Lehner, P.H. Nielsen, M. Schloter, P. Roslev and M. Wagner, *The Isotope Array, a New Tool That Employs Substrate-Mediated Labeling of rRNA for Determination of Microbial Community Structure and Function.* Appl. Environ. Microbiol., 2003. **69**(11): p. 6875-6887.
3. Ouverney, C.C. and J.A. Fuhrman, *Combined Microautoradiography-16S rRNA Probe Technique for Determination of Radioisotope Uptake by Specific Microbial Cell Types In Situ.* Appl. Environ. Microbiol., 1999. **65**(4): p. 1746-1752.
4. Jehmlich, N., F. Schmidt, M. Taubert, J. Seifert, F. Bastida, M. von Bergen, H.-H. Richnow and C. Vogt, *Protein-based stable isotope probing.* Nature Protocols, 2010. **5**(12): p. 1957-1966.
5. Murrell, J.C. and A.S. Whiteley, eds. *Stable Isotope Probing and Related Technologies*. 2011, ASM Press: Washington, D.C. 345.
6. Koch, B.J., T.A. McHugh, M. Hayer, E. Schwartz, S.J. Blazewicz, P. Dijkstra, N. van Gestel, J.C. Marks, R.L. Mau, E.M. Morrissey, J. Pett-Ridge and B.A. Hungate, *Estimating taxon-specific population dynamics in diverse microbial communities.* Ecosphere, 2018. **9**(1): p. e02090-15.
7. Hillion, F., B. Daigne, F. Girard and G. Slodzian, *A new high performance instrument: the CAMECA NanoSIMS 50*, in *Secondary Ion Mass Spectrometry: SIMS IX*, A. Benninghoven, et al., Editors. 1993, John Wiley & Sons: Chichester, UK. p. 254-257.
8. Ghosal, S., T.J. Leighton, K.E. Wheeler, I.D. Hutcheon and P.K. Weber, *Spatially resolved characterization of water and ion incorporation in Bacillus spores.* Applied and environmental microbiology, 2010. **76**(10): p. 3275-3282.
9. Orphan, V.J., C.H. House, K.-U. Hinrichs, K.D. McKeegan and E.F. DeLong, *Methane-consuming archaea revealed by directly coupled isotopic and phylogenetic analysis.* science, 2001. **293**(5529): p. 484-487.
10. Smart, K., M. Kilburn, C. Salter, J. Smith and C. Grovenor, *NanoSIMS and EPMA analysis of nickel localisation in leaves of the hyperaccumulator plant Alyssum lesbiacum.* International Journal of Mass Spectrometry, 2007. **260**(2-3): p. 107-114.
11. Stadermann, F.J., R.M. Walker and E. Zinner, *Nanosims: The next generation ion probe for the microanalysis of extraterrestrial material.* Meteoritics & Planetary Science, 1999. **34**: p. A111-A112.
12. Guerquin-Kern, J.-L., F. Hillion, J.-C. Madelmont, P. Labarre, J. Papon and A. Croisy, *Ultra-structural cell distribution of the melanoma marker iodobenzamide: improved potentiality of SIMS imaging in life sciences.* BioMedical Engineering OnLine, 2004: p. http://www.biomedical-engineering-online.com/content/3/1/10.
13. Kraft, M.L., S.F. Fishel, C.G. Marxer, P.K. Weber, I.D. Hutcheon and S.G. Boxer, *Quantitative analysis of supported membrane composition using the NanoSIMS.* Applied Surface Science, 2006. **252**(19): p. 6950-6956.
14. Moreau, J.W., P.K. Weber, M.C. Martin, B. Gilbert, I.D. Hutcheon and J.F. Banfield, *Extracellular proteins limit the dispersal of biogenic nanoparticles.* Science, 2007. **316**: p. 1600-1603.

15. Peteranderl, R. and C. Lechene, *Measure of carbon and nitrogen stable isotope ratios in cultured cells.* Journal of the American Society for Mass Spectrometry, 2004. **15**(4): p. 478-485.
16. Wainwright, M., P.K. Weber, J.B. Smith, I.D. Hutcheon, B. Klyce, N.C. Wickramasinghe, J.V. Narlikar and P. Rajaratnam, *Studies on bacteria-like particles sampled from the stratosphere.* Aeorobiologia, 2004. **20**: p. 237-240.
17. Galli Marxner, C., M.L. Kraft, P.K. Weber, I. Hutcheon and S.G. Boxer, *Supported membrane composition analysis by secondary ion mass spectrometry with high lateral resolution.* . Biophys J., 2005. **88**: p. 2965-2975.
18. Dekas, A.E., R.S. Poretsky and V.J. Orphan, *Deep-Sea Archaea Fix and Share Nitrogen in Methane-Consuming Microbial Consortia.* Science, 2009. **326**(5951): p. 422-426.
19. Halm, H., N. Musat, P. Lam, R. Langlois, F. Musat, S. Peduzzi, G. Lavik, C.J. Schubert, B. Sinha, J. LaRoche and M.M.M. Kuypers, *Co-occurrence of denitrification and nitrogen fixation in a meromictic lake, Lake Cadagno (Switzerland).* Environmental Microbiology, 2009. **11**(8): p. 2190-2190.
20. Musat, N., H. Halm, B. Winterholler, P. Hoppe, S. Peduzzi, F. Hillion, F. Horreard, R. Amann, B.B. Jørgensen and M.M.M. Kuypers, *A single-cell view on the ecophysiology of anaerobic phototrophic bacteria.* Proceedings of the National Academy of Sciences, 2008. **105**(46): p. 17861-17866.
21. Quintana, C., T.D. Wu, B. Delatour, M. Dhenain, J.L. Guerquin-Kern and A. Croisy, *Morphological and chemical studies of pathological human and mice brain at the subcellular level: Correlation between light, electron, and NanoSIMS microscopies.* Microscopy Research and Technique, 2007. **70**(4): p. 281-295.
22. Behrens, S., T. Losekann, J. Pett-Ridge, P.K. Weber, W. Ng, B.S. Stevenson, I.D. Hutcheon, D.A. Relman and A.M. Spormann, *Linking microbial phylogeny to metabolic activity at the single-cell level by using enhanced Element Labeling-catalyzed reporter deposition Fluorescence In Situ Hybridization (EL-FISH) and NanoSIMS.* Applied and Environmental Microbiology, 2008. **74**(10): p. 3143.
23. Finzi-Hart J. Pett-Ridge, J., P. Weber, R. Popa, S.J. Fallon, T. Gunderson, I. Hutcheon, K. Nealson and D.G. Capone, *Fixation and fate of carbon and nitrogen in Trichodesmium IMS101 using nanometer resolution secondary ion mass spectrometry (NanoSIMS).* PNAS, 2008. **106**: p. 6345-6350 *equal contribution.
24. Lechene, C., F. Hillion, G. McMahon, D. Benson, A. Kleinfeld, J.P. Kampf, D. Distel, Y. Luyten, J. Bonventre, D. Hentschel, K. Park, S. Ito, M. Schwartz, G. Benichou and G. Slodzian, *High-resolution quantitative imaging of mammalian and bacterial cells using stable isotope mass spectrometry.* Journal of Biology, 2006. **5**(6): p. 20.
25. Popa, R., P.K. Weber, J. Pett-Ridge, J.A. Finzi, S.J. Fallon, I.D. Hutcheon, K.H. Nealson and D.G. Capone, *Carbon and nitrogen fixation and metabolite exchange in and between individual cells of Anabaena oscillarioides.* Isme Journal, 2007. **1**(4): p. 354-360.
26. Ghosal, S., S.J. Fallon, T. Leighton, K.E. Wheeler, I.D. Hutcheon and P.K. Weber, *Imaging and 3D elemental characterization of intact bacterial spores with high-resolution secondary ion mass spectrometry (NanoSIMS) depth profile analysis.* Analytical Chemistry, 2008. **80**(15): p. 5986–5992.
27. Lechene, C.P., Y. Luyten, G. McMahon and D.L. Distel, *Quantitative imaging of nitrogen fixation by individual bacteria within animal cells.* Science, 2007. **317**: p. 1563-1566.

28. Herrmann, A., K. Ritz, N. Nunan, P. Clode, J. Pett-Ridge, M. Kilburn, D. Murphy, A. O'Donnell and E. Stockdale, *Nano-scale secondary ion mass spectrometry – a new analytical tool in biogeochemistry and soil ecology: A review article.* Soil Biology and Biochemistry, 2007. **39**: p. 1835-1850.
29. Mueller, C.W., P.K. Weber, M.R. Kilburn, C. Hoeschen, M. Kleber and J. Pett-Ridge, *Advances in the Analysis of Biogeochemical Interfaces: NanoSIMS to Investigate Soil Microenvironments*, in *Advances in Agronomy*, D. Sparks, Editor. 2013.
30. Renslow, R.S., S.R. Lindemann, J.K. Cole, Z. Zhu and C.R. Anderton, *Quantifying element incorporation in multispecies biofilms using nanoscale secondary ion mass spectrometry image analysis.* Biointerphases, 2016. **11**(2): p. 02A322.
31. Mayali, X., *NanoSIMS: microscale quantification of biogeochemical activity with large-scale impacts.* Annual Review of Marine Science, 2020. **12**: p. 449-467.
32. Gao, D., X. Huang and Y. Tao, *A critical review of NanoSIMS in analysis of microbial metabolic activities at single-cell level.* Critical reviews in biotechnology, 2016. **36**(5): p. 884-890.
33. Zhao, F.-J., K.L. Moore, E. Lombi and Y.-G. Zhu, *Imaging element distribution and speciation in plant cells.* Trends in plant science, 2014. **19**(3): p. 183-192.
34. Musat, N., F. Musat, P.K. Weber and J. Pett-Ridge, *Tracking microbial interactions with NanoSIMS.* Current opinion in biotechnology, 2016. **41**: p. 114-121.
35. Agüi-Gonzalez, P., S. Jähne and N.T. Phan, *SIMS imaging in neurobiology and cell biology.* Journal of Analytical Atomic Spectrometry, 2019. **34**(7): p. 1355-1368.
36. Boxer, S.G., M.L. Kraft and P.K. Weber, *Advances in imaging secondary ion mass spectrometry for biological samples.* Annual review of biophysics, 2009. **38**: p. 53-74.
37. Nuñez, J., R. Renslow, J.B. Cliff III and C.R. Anderton, *NanoSIMS for biological applications: current practices and analyses.* Biointerphases, 2018. **13**(3): p. 03B301.
38. Gorman, B.L. and M.L. Kraft, *High-Resolution Secondary Ion Mass Spectrometry Analysis of Cell Membranes*. 2019, ACS Publications.
39. CAMECA. *NanoSIMS 50L: Scientific Publications*. Available from: https://www.cameca.com/products/sims/nanosims.
40. Pett-Ridge, J. and P.K. Weber, *NanoSIP: NanoSIMS applications for microbial biology*, in *Microbial Systems Biology: Methods and Protocols*, A. Navid, Editor. 2012, Humana Press, **Cover Image**.
41. Dekas, A.E., A.E. Parada, X. Mayali, J.A. Fuhrman, J. Wollard, P.K. Weber and J. Pett-Ridge, *Characterizing chemoautotrophy and heterotrophy in marine archaea and bacteria with single-cell multi-isotope nanoSIP.* Frontiers in Microbiology, 2019. **10**(2682).
42. Chadwick, G.L., F.J. Otero, J.A. Gralnick, D.R. Bond and V.J. Orphan, *NanoSIMS imaging reveals metabolic stratification within current-producing biofilms.* Proceedings of the National Academy of Sciences, 2019. **116**(41): p. 20716-20724.
43. Volland, J.-M., A. Schintlmeister, H. Zambalos, S. Reipert, P. Mozetič, S. Espada-Hinojosa, V. Turk, M. Wagner and M. Bright, *NanoSIMS and tissue autoradiography reveal symbiont carbon fixation and organic carbon transfer to giant ciliate host.* The ISME journal, 2018. **12**(3): p. 714-727.
44. Calabrese, F., I. Voloshynovska, F. Musat, M. Thullner, M. Schlömann, H.H. Richnow, J. Lambrecht, S. Müller, L.Y. Wick and N. Musat, *Quantitation and comparison of*

phenotypic heterogeneity among single cells of monoclonal microbial populations. Frontiers in microbiology, 2019. **10**: p. 2814.
45. Braun, P.D., H.N. Schulz-Vogt, A. Vogts and M. Nausch, *Differences in the accumulation of phosphorus between vegetative cells and heterocysts in the cyanobacterium Nodularia spumigena.* Scientific reports, 2018. **8**(1): p. 1-6.
46. Gross, A., Y. Lin, P.K. Weber, J. Pett-Ridge and W.L. Silver, *The role of soil redox conditions in microbial phosphorus cycling in humid tropical forests.* Ecology, 2020. **101**(2): p. e02928.
47. Ackerman, C.M., P.K. Weber, T. Xiao, B. Thai, T.J. Kuo, E. Zhang, J. Pett-Ridge and C.J. Chang, *Multimodal LA-ICP-MS and nanoSIMS imaging enables copper mapping within photoreceptor megamitochondria in a zebrafish model of Menkes disease.* Metallomics, 2018. **10**(3): p. 474-485.
48. Hong-Hermesdorf, A., M. Miethke, S.D. Gallaher, J. Kropat, S.C. Dodani, D. Barupala, J. Chan, D.W. Domaille, D.I. Shirasaki, J.A. Loo, P.K. Weber, J. Pett-Ridge, T.L. Stemmler, C.J. Chang and S.S. Merchant., *Selective sub-cellular visualization of trace metals identifies dynamic sites of Cu accumulation in Chlamydomonas.* Nature Chemical Biology, 2014. **10**: p. 1034-1042
49. Dawson, K.S., S. Scheller, J.G. Dillon and V.J. Orphan, *Stable isotope phenotyping via cluster analysis of NanoSIMS data as a method for characterizing distinct microbial ecophysiologies and sulfur-cycling in the environment.* Frontiers in microbiology, 2016. **7**: p. 774.
50. Berry, D., E. Mader, T.K. Lee, D. Woebken, Y. Wang, D. Zhu, M. Palatinszky, A. Schintlmeister, M.C. Schmid and B.T. Hanson, *Tracking heavy water (D2O) incorporation for identifying and sorting active microbial cells.* Proceedings of the National Academy of Sciences, 2015. **112**(2): p. E194-E203.
51. Kopf, S.H., S.E. McGlynn, A. Green-Saxena, Y. Guan, D.K. Newman and V.J. Orphan, *Heavy water and 15 N labelling with N ano SIMS analysis reveals growth rate-dependent metabolic heterogeneity in chemostats.* Environmental microbiology, 2015. **17**(7): p. 2542-2556.
52. Ploug, H., N. Musat, B. Adam, C.L. Moraru, G. Lavik, T. Vagner, B. Bergman and M.M.M. Kuypers, *Carbon and nitrogen fluxes associated with the cyanobacterium Aphanizomenon sp. in the Baltic Sea.* ISME J, 2010. **4**(9): p. 1215-1223.
53. Scheller, S., H. Yu, G.L. Chadwick, S.E. McGlynn and V.J. Orphan, *Artificial electron acceptors decouple archaeal methane oxidation from sulfate reduction.* Science, 2016. **351**(6274): p. 703-707.
54. Dekas, A.E., S.A. Connon, G.L. Chadwick, E. Trembath-Reichert and V.J. Orphan, *Activity and interactions of methane seep microorganisms assessed by parallel transcription and FISH-NanoSIMS analyses.* ISME J, 2016. **10**(3): p. 678-692.
55. Green-Saxena, A., A.E. Dekas, N.F. Dalleska and V.J. Orphan, *Nitrate-based niche differentiation by distinct sulfate-reducing bacteria involved in the anaerobic oxidation of methane.* ISME J, 2014. **8**(1): p. 150-163.
56. Milucka, J., M. Kirf, L. Lu, A. Krupke, P. Lam, S. Littmann, M.M.M. Kuypers and C.J. Schubert, *Methane oxidation coupled to oxygenic photosynthesis in anoxic waters.* ISME J, 2015. **9**(9): p. 1991-2002.

57. Marlow, J.J., J.A. Steele, W. Ziebis, A.R. Thurber, L.A. Levin and V.J. Orphan, *Carbonate-hosted methanotrophy represents an unrecognized methane sink in the deep sea.* Nature Communications, 2014. **5**(1): p. 1-12.
58. Oswald, K., J.S. Graf, S. Littmann, D. Tienken, A. Brand, B. Wehrli, M. Albertsen, H. Daims, M. Wagner and M.M. Kuypers, *Crenothrix are major methane consumers in stratified lakes.* The ISME journal, 2017. **11**(9): p. 2124-2140.
59. Foster, R.A., M.M. Kuypers, T. Vagner, R.W. Paerl, N. Musat and J.P. Zehr, *Nitrogen fixation and transfer in open ocean diatom-cyanobacterial symbioses.* Isme J, 2011. **5**(9): p. 1484-93.
60. Thompson, A.W., R.A. Foster, A. Krupke, B.J. Carter, N. Musat, D. Vaulot, M.M.M. Kuypers and J.P. Zehr, *Unicellular Cyanobacterium Symbiotic with a Single-Celled Eukaryotic Alga.* Science, 2012. **337**(6101): p. 1546-1550.
61. Adam, B., I. Klawonn, J.B. Sveden, J. Bergkvist, N. Nahar, J. Walve, S. Littmann, M.J. Whitehouse, G. Lavik, M.M.M. Kuypers and H. Ploug, *N2-fixation, ammonium release and N-transfer to the microbial and classical food web within a plankton community.* ISME J, 2016. **10**(2): p. 450-459.
62. Berry, D., B. Stecher, A. Schintlmeister, J. Reichert, S. Brugiroux, B. Wild, W. Wanek, A. Richter, I. Rauch and T. Decker, *Host-compound foraging by intestinal microbiota revealed by single-cell stable isotope probing.* Proceedings of the National Academy of Sciences, 2013. **110**(12): p. 4720-4725.
63. Carpenter, K.J., P.K. Weber, M.L. Davisson, J. Pett-Ridge, M.I. Haverty and P.J. Keeling, *Correlated SEM, FIB-SEM, TEM, and NanoSIMS Imaging of Microbes from the Hindgut of a Lower Termite: Methods for In Situ Functional and Ecological Studies of Uncultivable Microbes.* Microscopy and Microanalysis, 2013. **19**(06): p. 1490-1501.
64. Tai, V., K.J. Carpenter, P.K. Weber, C.A. Nalepa, S.J. Perlman and P.J. Keeling, *Genome evolution and nitrogen-fixation in bacterial ectosymbionts of a protist inhabiting wood-feeding cockroaches.* Applied and Environmental Microbiology, 2016. **doi:10.1128/AEM.00611-16**
65. Ceh, J., M.R. Kilburn, J.B. Cliff, J.B. Raina, M. van Keulen and D.G. Bourne, *Nutrient cycling in early coral life stages: Pocillopora damicornis larvae provide their algal symbiont (Symbiodinium) with nitrogen acquired from bacterial associates.* Ecology and Evolution, 2013. **3**(8): p. 2393-2400.
66. Pernice, M., S.R. Dunn, L. Tonk, S. Dove, I. Domart-Coulon, P. Hoppe, A. Schintlmeister, M. Wagner and A. Meibom, *A nanoscale secondary ion mass spectrometry study of dinoflagellate functional diversity in reef-building corals.* Environmental microbiology, 2015. **17**(10): p. 3570-3580.
67. Wangpraseurt, D., M. Pernice, P. Guagliardo, M.R. Kilburn, P.L. Clode, L. Polerecky and M. Kühl, *Light microenvironment and single-cell gradients of carbon fixation in tissues of symbiont-bearing corals.* The ISME journal, 2016. **10**(3): p. 788-792.
68. Lema, K.A., P.L. Clode, M.R. Kilburn, R. Thornton, B.L. Willis and D.G. Bourne, *Imaging the uptake of nitrogen-fixing bacteria into larvae of the coral Acropora millepora.* The ISME journal, 2016. **10**(7): p. 1804-1808.
69. Kopp, C., I. Domart-Coulon, D. Barthelemy and A. Meibom, *Nutritional input from dinoflagellate symbionts in reef-building corals is minimal during planula larval life stage.* Science advances, 2016. **2**(3): p. e1500681.

70. Yang, S.-H., K. Tandon, C.-Y. Lu, N. Wada, C.-J. Shih, S.S.-Y. Hsiao, W.-N. Jane, T.-C. Lee, C.-M. Yang and C.-T. Liu, *Metagenomic, phylogenetic, and functional characterization of predominant endolithic green sulfur bacteria in the coral Isopora palifera.* Microbiome, 2019. **7**(1): p. 1-13.
71. Samo, T.J., J.A. Kimbrel, D.J. Nilson, J. Pett-Ridge, P.K. Weber and X. Mayali, *Attachment between heterotrophic bacteria and microalgae influences symbiotic microscale interactions.* Environmental microbiology, 2018.
72. de-Bashan, L.E., X. Mayali, B.M. Bebout, P.K. Weber, A.M. Detweiler, J.-P. Hernandez, L. Prufert-Bebout and Y. Bashan, *Establishment of stable synthetic mutualism without co-evolution between microalgae and bacteria demonstrated by mutual transfer of metabolites (NanoSIMS isotopic imaging) and persistent physical association (Fluorescent in situ hybridization).* Algal Research, 2016. **15**: p. 179-186.
73. Alonso, C., N. Musat, B. Adam, M. Kuypers and R. Amann, *HISH–SIMS analysis of bacterial uptake of algal-derived carbon in the Río de la Plata estuary.* Systematic and applied microbiology, 2012. **35**(8): p. 541-548.
74. Leroy, C., A. Jauneau, Y. Martinez, A. Cabin-Flaman, D. Gibouin, J. Orivel and N. Séjalon-Delmas, *Exploring fungus–plant N transfer in a tripartite ant–plant–fungus mutualism.* Annals of botany, 2017. **120**(3): p. 417-426.
75. Lee, J.Z., L.C. Burow, D. Woebken, R.C. Everroad, M.D. Kubo, A.M. Spormann, P.K. Weber, J. Pett-Ridge, B.M. Bebout and T.M. Hoehler, *Fermentation couples Chloroflexi and sulfate-reducing bacteria to Cyanobacteria in hypersaline microbial mats.* Frontiers in Microbiology, 2014. **5**.
76. Nuccio, E.E., A. Hodge, J. Pett-Ridge, D.J. Herman, P.K. Weber and M.K. Firestone, *An arbuscular mycorrhizal fungus significantly modifies the soil bacterial community and nitrogen cycling during litter decomposition.* Environmental Microbiology, 2013. **15**(6): p. 1870-1881, **Cover Image**.
77. Kaiser, C., M.R. Kilburn, P.L. Clode, L. Fuchslueger, M. Koranda, J.B. Cliff, Z.M. Solaiman and D.V. Murphy, *Exploring the transfer of recent plant photosynthates to soil microbes: mycorrhizal pathway vs direct root exudation.* New Phytologist, 2015. **205**(4): p. 1537-1551.
78. Kuga, Y., N. Sakamoto and H. Yurimoto, *Stable isotope cellular imaging reveals that both live and degenerating fungal pelotons transfer carbon and nitrogen to orchid protocorms.* New Phytologist, 2014. **202**(2): p. 594-605.
79. Pett-Ridge, J. and M.K. Firestone, *Using stable isotopes to explore root-microbe-mineral interactions in soil.* Rhizosphere, 2017. **3**: p. 244-253.
80. Hestrin, R., E.C. Hammer, C.W. Mueller and J. Lehmann, *Synergies between mycorrhizal fungi and soil microbial communities increase plant nitrogen acquisition.* Communications biology, 2019. **2**(1): p. 1-9.
81. Gorka, S., M. Dietrich, W. Mayerhofer, R. Gabriel, J. Wiesenbauer, V. Martin, Q. Zheng, B. Imai, J. Prommer and M. Weidinger, *Rapid transfer of plant photosynthates to soil bacteria via ectomycorrhizal hyphae and its interaction with nitrogen availability.* Frontiers in microbiology, 2019. **10**: p. 168.
82. Worrich, A., H. Stryhanyuk, N. Musat, S. König, T. Banitz, F. Centler, K. Frank, M. Thullner, H. Harms and H.-H. Richnow, *Mycelium-mediated transfer of water and nutrients stimulates bacterial activity in dry and oligotrophic environments.* Nature communications, 2017. **8**(1): p. 1-9.

83. Bougoure, J., M. Ludwig, M. Brundrett, J. Cliff, P. Clode, M. Kilburn and P. Grierson, *High-resolution secondary ion mass spectrometry analysis of carbon dynamics in mycorrhizas formed by an obligately myco-heterotrophic orchid.* Plant, Cell & Environment, 2014. **37**(5): p. 1223-1230.
84. Hill, P.W., R. Broughton, J. Bougoure, W. Havelange, K.K. Newsham, H. Grant, D.V. Murphy, P. Clode, S. Ramayah and K.A. Marsden, *Angiosperm symbioses with non-mycorrhizal fungal partners enhance N acquisition from ancient organic matter in a warming maritime Antarctic.* Ecology letters, 2019. **22**(12): p. 2111-2119.
85. Mergelov, N., C.W. Mueller, I. Prater, I. Shorkunov, A. Dolgikh, E. Zazovskaya, V. Shishkov, V. Krupskaya, K. Abrosimov and A. Cherkinsky, *Alteration of rocks by endolithic organisms is one of the pathways for the beginning of soils on Earth.* Scientific reports, 2018. **8**(1): p. 1-15.
86. Kopittke, P.M., R.C. Dalal, C. Hoeschen, C. Li, N.W. Menzies and C.W. Mueller, *Soil organic matter is stabilized by organo-mineral associations through two key processes: The role of the carbon to nitrogen ratio.* Geoderma, 2020. **357**: p. 113974.
87. Keiluweit, M., J.J. Bougoure, L.H. Zeglin, D.D. Myrold, P.K. Weber, J. Pett-Ridge, M. Kleber and P.S. Nico, *Nano-scale investigation of the association of microbial nitrogen residues with iron (hydr)oxides in a forest soil O-horizon.* Geochimica et Cosmochimica Acta, 2012. **95**(0): p. 213-226.
88. Keiluweit, M., J.J. Bougoure, P.S. Nico, J. Pett-Ridge, P.K. Weber and M. Kleber, *Mineral protection of soil carbon counteracted by root exudates.* Nature Climate Change, 2015. **5**(6): p. 588-595.
89. Morrison, K.D., R. Misra and L.B. Williams, *Unearthing the antibacterial mechanism of medicinal clay: A geochemical approach to combating antibiotic resistance.* Scientific Reports, 2016. **6**: p. 19043.
90. Londono, S.C., H.E. Hartnett and L.B. Williams, *Antibacterial activity of aluminum in clay from the Colombian Amazon.* Environmental Science & Technology, 2017. **51**(4): p. 2401-2408.
91. Eichorst, S.A., F. Strasser, T. Woyke, A. Schintlmeister, M. Wagner and D. Woebken, *Advancements in the application of NanoSIMS and Raman microspectroscopy to investigate the activity of microbial cells in soils.* FEMS Microbiology Ecology, 2015. **91**(10).
92. Pasulka, A.L., K. Thamatrakoln, S.H. Kopf, Y. Guan, B. Poulos, A. Moradian, M.J. Sweredoski, S. Hess, M.B. Sullivan and K.D. Bidle, *Interrogating marine virus-host interactions and elemental transfer with BONCAT and nanoSIMS-based methods.* Environmental microbiology, 2018. **20**(2): p. 671-692.
93. Greenwood, D.J., M.S. Dos Santos, S. Huang, M.R. Russell, L.M. Collinson, J.I. MacRae, A. West, H. Jiang and M.G. Gutierrez, *Subcellular antibiotic visualization reveals a dynamic drug reservoir in infected macrophages.* Science, 2019. **364**(6447): p. 1279-1282.
94. Gates, S.D., R.C. Condit, N. Moussatche, B.J. Stewart, A.J. Malkin and P.K. Weber, *High initial sputter rate found for vaccinia virions using isotopic labeling, nanoSIMS, and AFM.* Analytical chemistry, 2018. **90**(3): p. 1613-1620.
95. Stuart, R.K., X. Mayali, A.A. Boaro, A. Zemla, R.C. Everroad, D. Nilson, P.K. Weber, M. Lipton, B.M. Bebout and J. Pett-Ridge, *Light Regimes Shape Utilization of*

Extracellular Organic C and N in a Cyanobacterial Biofilm. mBio, 2016. **7**(3): p. e00650-16.
96. Stuart, R.K., X. Mayali, J.Z. Lee, R.C. Everroad, M. Hwang, B.M. Bebout, P.K. Weber, J. Pett-Ridge and M.P. Thelen, *Cyanobacterial reuse of extracellular organic carbon in microbial mats.* ISME J, 2016. **10**(5): p. 1240-1251.
97. Stuart, R.K., X. Mayali, M.P. Thelen, J. Pett-Ridge and P.K. Weber, *Measuring Cyanobacterial Metabolism in Biofilms with NanoSIMS Isotope Imaging and Scanning Electron Microscopy (SEM).* Bioprotocol, 2017. **7**: p. e2263.
98. Probst, A.J., T. Weinmaier, K. Raymann, A. Perras, J.B. Emerson, T. Rattei, G. Wanner, A. Klingl, I.A. Berg, M. Yoshinaga, B. Viehweger, K.-U. Hinrichs, B.C. Thomas, S. Meck, A.K. Auerbach, M. Heise, A. Schintlmeister, M. Schmid, M. Wagner, S. Gribaldo, J.F. Banfield, and C. Moissl-Eichinger, *Biology of a widespread uncultivated archaeon that contributes to carbon fixation in the subsurface.* Nat Commun, 2014. **5**.
99. Tveit, A.T., A.G. Hestnes, S.L. Robinson, A. Schintlmeister, S.N. Dedysh, N. Jehmlich, M. von Bergen, C. Herbold, M. Wagner and A. Richter, *Widespread soil bacterium that oxidizes atmospheric methane.* Proceedings of the National Academy of Sciences, 2019. **116**(17): p. 8515-8524.
100. Sheik, A.R., E.E. Muller, J.-N. Audinot, L.A. Lebrun, P. Grysan, C. Guignard and P. Wilmes, *In situ phenotypic heterogeneity among single cells of the filamentous bacterium Candidatus Microthrix parvicella.* The ISME journal, 2016. **10**(5): p. 1274-1279.
101. Nikolic, N., F. Schreiber, D.J. Kiviet, T. Bergmiller, S. Littmann, M.M. Kuypers and M. Ackermann, *Cell-to-cell variation and specialization in sugar metabolism in clonal bacterial populations.* PLoS genetics, 2017. **13**(12): p. e1007122.
102. Gangwe Nana, G.Y., C. Ripoll, A. Cabin-Flaman, D. Gibouin, A. Delaune, L. Jannière, G. Grancher, G. Chagny, C. Loutelier-Bourhis and E. Lentzen, *Division-based, growth rate diversity in bacteria.* Frontiers in microbiology, 2018. **9**: p. 849.
103. Zimmermann, M., S. Escrig, T. Hübschmann, M.K. Kirf, A. Brand, R.F. Inglis, N. Musat, S. Müller, A. Meibom and M. Ackermann, *Phenotypic heterogeneity in metabolic traits among single cells of a rare bacterial species in its natural environment quantified with a combination of flow cell sorting and NanoSIMS.* Frontiers in microbiology, 2015. **6**: p. 243.
104. Tsednee, M., M. Castruita, P.A. Salomé, A. Sharma, B.E. Lewis, S.R. Schmollinger, D. Strenkert, K. Holbrook, M.S. Otegui and K. Khatua, *Manganese co-localizes with calcium and phosphorus in Chlamydomonas acidocalcisomes and is mobilized in manganese-deficient conditions.* Journal of Biological Chemistry, 2019. **294**(46): p. 17626-17641.
105. Kessler, N., R. Armoza-Zvuloni, S. Wang, S. Basu, P.K. Weber, R.K. Stuart and Y. Shaked, *Selective collection of iron-rich dust particles by natural Trichodesmium colonies.* The ISME journal, 2020. **14**(1): p. 91-103.
106. Newsome, L., R. Lopez Adams, H.F. Downie, K.L. Moore and J.R. Lloyd, *NanoSIMS imaging of extracellular electron transport processes during microbial iron (III) reduction.* FEMS microbiology ecology, 2018. **94**(8): p. fiy104.
107. Fleming, E., T. Woyke, R. Donatello, M.M. Kuypers, A. Sczyrba, S. Littmann and D. Emerson, *Insights into the fundamental physiology of the uncultured Fe-oxidizing bacterium Leptothrix ochracea.* Applied and Environmental Microbiology, 2018. **84**(9).

108. Stryhanyuk, H., F. Calabrese, S. Kümmel, F. Musat, H.H. Richnow and N. Musat, *Calculation of single cell assimilation rates from SIP-NanoSIMS-derived isotope ratios: a comprehensive approach.* Frontiers in microbiology, 2018. **9**: p. 2342.
109. Arandia-Gorostidi, N., P.K. Weber, L. Alonso-Saez, X.A.G. Moran and X. Mayali, *Elevated temperature increases carbon and nitrogen fluxes between phytoplankton and heterotrophic bacteria through physical attachment.* ISME J, 2017. **11**(3): p. 641-650.
110. Frisz, J.F., K. Lou, H.A. Klitzing, W.P. Hanafin, V. Lizunov, R.L. Wilson, K.J. Carpenter, R. Kim, I.D. Hutcheon and J. Zimmerberg, *Direct chemical evidence for sphingolipid domains in the plasma membranes of fibroblasts.* Proceedings of the National Academy of Sciences, 2013. **110**(8): p. E613-E622.
111. Smith, N.S., R.W. Boswell, P.P. Tesch and N.P. Martin, *Rf system, magnetic filter, and high voltage isolation for an inductively coupled plasma ion source*. 2017, Google Patents.
112. Smith, N., P. Tesch, N. Martin and D. Kinion, *A high brightness source for nano-probe secondary ion mass spectrometry.* Applied surface science, 2008. **255**(4): p. 1606-1609.
113. Malherbe, J., F. Penen, M.-P. Isaure, J. Frank, G. Hause, D. Dobritzsch, E. Gontier, F.o. Horréard, F.o. Hillion and D. Schaumlöffel, *A new radio frequency plasma oxygen primary ion source on nano secondary ion mass spectrometry for improved lateral resolution and detection of electropositive elements at single cell level.* Analytical chemistry, 2016. **88**(14): p. 7130-7136.
114. Cabin-Flaman, A., A.-F.o. Monnier, Y. Coffinier, J.-N. Audinot, D. Gibouin, T. Wirtz, R. Boukherroub, H.-N.l. Migeon, A. Bensimon and L. Jannière, *Combed single DNA molecules imaged by secondary ion mass spectrometry.* Analytical chemistry, 2011. **83**(18): p. 6940-6947.
115. Cabin-Flaman, A., A.-F. Monnier, Y. Coffinier, J.-N. Audinot, D. Gibouin, T. Wirtz, R. Boukherroub, H.-N. Migeon, A. Bensimon and L. Jannière, *Combining combing and secondary ion mass spectrometry to study DNA on chips using 13C and 15N labeling.* F1000Research, 2016. **5**.
116. Weber, P.K., G.A. Graham, N.E. Teslich, W. MoberlyChan, S. Ghosal, T.J. Leighton and K.E. Wheeler, *NanoSIMS imaging of Bacillus spores sectioned by Focused Ion Beam.* Journal of Microscopy, 2010. **238**: p. 189-199.
117. Wilson, R.G., F.A. Stevie and C.W. Magee, *Secondary Ion Mass Spectrometry: A Practical Handbook for Depth Profiling and Bulk Impurity Analysis*. 1989, New York: Wiley.
118. Polerecky, L., B. Adam, J. Milucka, N. Musat, T. Vagner and M.M. Kuypers, *Look@ NanoSIMS–a tool for the analysis of nanoSIMS data in environmental microbiology.* Environmental microbiology, 2012. **14**(4): p. 1009-1023.
119. Huang, W., K.E. Hammel, J. Hao, A. Thompson, V.I. Timokhin and S.J. Hall, *Enrichment of lignin-derived carbon in mineral-associated soil organic matter.* Environmental science & technology, 2019. **53**(13): p. 7522-7531.
120. Whitman, T., Z. Zhu and J. Lehmann, *Carbon mineralizability determines interactive effects on mineralization of pyrogenic organic matter and soil organic carbon.* Environmental science & technology, 2014. **48**(23): p. 13727-13734.
121. Hatton, P.-J., L. Remusat, B. Zeller, E.A. Brewer and D. Derrien, *NanoSIMS investigation of glycine-derived C and N retention with soil organo-mineral associations.* Biogeochemistry, 2015. **125**(3): p. 303-313.

122. Li, T., T.D. Wu, L. Mazeas, L. Toffin, J.L. Guerquin-Kern, G. Leblon and T. Bouchez, *Simultaneous analysis of microbial identity and function using NanoSIMS.* Environmental Microbiology, 2008. **10**(3): p. 580-588.
123. Benn, P.A. and M.A. Perle, *Chapter 4.Chromosome staining and banding techniques.*, in *Human Cytogenetics: Volume I, Constitutional Analysis: A Practical Approach*, D.E. Rooney and B.H. Czepulkowski, Editors. 1992, Oxford University Press: New York.
124. Latt, S.A., *Microfluorometric detection of deoxyribonucleic acid replication in human metaphase chromosomes.* Proc Natl Acad Sci USA, 1973. **49**: p. 3395-3399.
125. Manefield, M., A.S. Whiteley, R.I. Griffiths and M.J. Bailey, *RNA stable isotope probing, a novel means of linking microbial community function to phylogeny.* Applied and Environmental Microbiology, 2002. **68**: p. 5367-5373.
126. Radajewski, S., P. Ineson, N.R. Parekh and J. Murrell, *Stable-isotope probing as a tool in microbial ecology.* Nature, 2000. **403**(10): p. 646-649.
127. Jensen, L.H.S., T. Cheng, F.O.V. Plane, S. Escrig, A. Comment, B. van den Brandt, B.M. Humbel and A. Meibom. *En route to ion microprobe analysis of soluble compounds at the single cell level: The CryoNanoSIMS*. in *European Microscopy Congress 2016: Proceedings*. 2016. Wiley Online Library.
128. Lovrić, J., P. Malmberg, B.R. Johansson, J.S. Fletcher and A.G. Ewing, *Multimodal imaging of chemically fixed cells in preparation for NanoSIMS.* Analytical chemistry, 2016. **88**(17): p. 8841-8848.
129. Gibbin, E., A. Gavish, I. Domart-Coulon, E. Kramarsky-Winter, O. Shapiro, A. Meibom and A. Vardi, *Using NanoSIMS coupled with microfluidics to visualize the early stages of coral infection by Vibrio coralliilyticus.* BMC microbiology, 2018. **18**(1): p. 1-10.
130. Nunan, N., K. Ritz, D. Crabb, K. Harris, K. Wu, J.W. Crawford and I.M. Young, *Quantification of the in situ distribution of soil bacteria by large-scale imaging of thin sections of undisturbed soil.* FEMS Microbiology Ecology, 2001. **37**(1): p. 67-77.
131. Kuo, J., ed. *Electron Microscopy: Methods and Protocols*. 2nd edition ed. Methods in Molecular Biology. 2007, Humana Press: Totowa, NJ.
132. Tippkötter, R. and K. Ritz, *Evaluation of polyester, epoxy and acrylic resins for suitability in preparation of soil thin sections for in situ biological studies.* Geoderma, 1996. **69**(1-2): p. 31-57.
133. Chandra, S. and G.H. Morrison, *Sample preparation of animal tissues and cell cultures for secondary ion mass spectrometry (SIMS) microscopy.* Biology of the Cell, 1992. **74**: p. 31-42.
134. Dykstra, M.J. and L.E. Reuss, eds. *Biological Electron Microscopy: Theory, Techniques and Troubleshooting*. 2nd ed. 2003, Kluwer Academic/Plenum Publishers: New York.
135. Echlin, P., *Low-Temperature Microscopy and Analysis*. 1992, New York: Springer.
136. Musat, N., H. Stryhanyuk, P. Bombach, L. Adrian, J.-N. Audinot and H.H. Richnow, *The effect of FISH and CARD-FISH on the isotopic composition of 13C- and 15N-labeled Pseudomonas putida cells measured by nanoSIMS.* Systematic and Applied Microbiology, 2014. **37**(4): p. 267-276.
137. Woebken, D., L.C. Burow, F. Behnam, X. Mayali, A. Schintlmeister, E.D. Fleming, L. Prufert-Bebout, S.W. Singer, A. Lopez Cortes, T.M. Hoehler, J. Pett-Ridge, A.M. Spormann, M. Wagner, P.K. Weber and B.M. Bebout, *Revisiting N-2 fixation in Guerrero Negro intertidal microbial mats with a functional single-cell approach.* Isme Journal, 2015. **9**(2): p. 485-496.

138. Herrmann, A.M., P.L. Clode, I.R. Fletcher, N. Nunan, E.A. Stockdale, A.G. O'Donnel and D.V. Murphy, *A novel method for the study of the biophysical interface in soils using nano-scale secondary ion mass spectrometry.* Rapid Communications in Mass Spectrometry, 2007. **21**(1): p. 29-34.
139. Weng, N., H. Jiang and W.-X. Wang, *In situ subcellular imaging of copper and zinc in contaminated oysters revealed by nanoscale secondary ion mass spectrometry.* Environmental science & technology, 2017. **51**(24): p. 14426-14435.
140. Rogge, A., C.M. Flintrop, M.H. Iversen, I. Salter, A.A. Fong, A. Vogts and A.M. Waite, *Hard and soft plastic resin embedding for single-cell element uptake investigations of marine-snow-associated microorganisms using nano-scale secondary ion mass spectrometry.* Limnology and Oceanography: Methods, 2018. **16**(8): p. 484-503.
141. Fike, D.A., C.L. Gammon, W. Ziebis and V.J. Orphan, *Micron-scale mapping of sulfur cycling across the oxycline of a cyanobacterial mat: a paired nanoSIMS and CARD-FISH approach.* ISME Journal, 2008. **2**(7): p. 749-759.
142. De Gregorio, B.T., R.M. Stroud, L.R. Nittler, C.M.O.D. Alexander, A.L.D. Kilcoyne and T.J. Zega, *Isotopic anomalies in organic nanoglobules from Comet 81P/Wild 2: Comparison to Murchison nanoglobules and isotopic anomalies induced in terrestrial organics by electron irradiation.* Geochimica et Cosmochimica Acta, 2010. **74**(15): p. 4454-4470.
143. Lehmann, J., B.Q. Liang, D. Solomon, M. Lerotic, F. Luiza˜ o, J. Kinyangi, T. Scha¨ fer, S. Wirick and C. Jacobsen, *Near-edge X-ray absorption fine structure (NEXAFS) spectroscopy for mapping nano-scale distribution of organic carbon forms in soil: application to black carbon particles.* Global Biogeochemical Cycles, 2005. **29**: p. Art. No. GB1013.
144. Flynn, G.J., L.P. Keller, C. Jacobsen and S. Wirick, *An assessment of the amount and types of organic matter contributed to the Earth by interplanetary dust.* Advances in Space Research, 2004. **33**: p. 57-66.
145. Gnaser, H., *Formation of metastable N2- and CO- anions in sputtering.* Physical Review A, 1997. **56**(4): p. R2518.
146. McMahon, G., H.F. Saint-Cyr, C. Lechene and C.J. Unkefer, *CN- Secondary Ions Form by Recombination as Demonstrated Using Multi-Isotope Mass Spectrometry of 13C- and 15N-Labeled Polyglycine.* Journal of the American Society for Mass Spectrometry, 2006. **17**(8): p. 1181-1187.
147. Mayali, X., P.K. Weber, E. Nuccio, J. Lietard, M. Somoza, S.J. Blazewicz and J. Pett-Ridge, *Chip-SIP: Stable Isotope Probing Analyzed with rRNA-Targeted Microarrays and NanoSIMS,* in *Stable Isotope Probing*. 2019, Springer. p. 71-87.
148. Gnaser, H., *Singly-and doubly-negative carbon clusters in sputtering: Energy spectra, abundance distributions and unimolecular fragmentation.* Nuclear Instruments and Methods in Physics Research Section B: Beam Interactions with Materials and Atoms, 1999. **149**(1-2): p. 38-52.
149. Weber, P.K., C.R. Bacon, I.D. Hutcheon, B.L. Ingram and J.L. Wooden, *Ion microprobe measurement of strontium isotopes in calcium carbonate with application to salmon otoliths.* Geochimica et Cosmochimica Acta, 2005. **69**(5): p. 1225-1239.
150. Ghosal, S., S.J. Fallon, T. Leighton, K. Wheeler, I.D. Hutcheon and P.K. Weber, *Analysis of bacterial spore permeability to water and ions using NanoSecondary Ion Mass*

Spectrometry (NanoSIMS). Abstracts of Papers of the American Chemical Society, 2006. **231**.
151. Wolfe-Simon, F., J.S. Blum, T.R. Kulp, G.W. Gordon, S.E. Hoeft, J. Pett-Ridge, J.F. Stolz, S.M. Webb, P.K. Weber, P.C.W. Davies, A.D. Anbar and R.S. Oremland, *A bacterium that can grow by using arsenic instead of phosphorus.* Science, 2011.
152. Hauri, E.H., D. Papineau, J. Wang and F. Hillion, *High-precision analysis of multiple sulfur isotopes using NanoSIMS.* Chemical Geology, 2016. **420**: p. 148-161.
153. Chandra, S., D.R. Smith and G.H. Morrison, *Subcellular imaging by dynamic SIMS ion microscopy.* Anal Chem, 2000. **72**: p. 104A - 114A.
154. Guerquin-Kern, J.L., T.D. Wu, C. Quintana and A. Croisy, *Progress in analytical imaging of the cell by dynamic secondary ion mass spectrometry (SIMS microscopy).* Biochimica Et Biophysica Acta-General Subjects, 2005. **1724**(3): p. 228-238.
155. Burns, M.S., D.M. File, V. Deline and P. Galle, *Matrix effects in secondary ion mass spectrometric analysis of biological tissue.* Scanning electron microscopy, 1986(Pt 4): p. 1277-1290.
156. Harris, W.C., S. Chandra and G.H. Morrison, *Ion implantation for quantitative ion microscopy of biological soft tissue.* Analytical chemistry, 1983. **55**(12): p. 1959-1963.
157. Phinney, D., *Quantitative Analysis of Microstructures by Secondary Ion Mass Spectrometry.* Microscopy and Microanalysis, 2006. **12**(4): p. 352.
158. Decelle, J., G. Veronesi, B. Gallet, H. Stryhanyuk, P. Benettoni, M. Schmidt, R. Tucoulou, M. Passarelli, S. Bohic and P. Clode, *Subcellular Chemical Imaging: New Avenues in Cell Biology.* Trends in Cell Biology, 2020. **30**(3): p. 173-188.
159. Penen, F., J. Malherbe, M.-P. Isaure, D. Dobritzsch, I. Bertalan, E. Gontier, P. Le Coustumer and D. Schaumlöffel, *Chemical bioimaging for the subcellular localization of trace elements by high contrast TEM, TEM/X-EDS, and NanoSIMS.* Journal of Trace Elements in Medicine and Biology, 2016. **37**: p. 62-68.
160. Nomaki, H., C. LeKieffre, S. Escrig, A. Meibom, S. Yagyu, E.A. Richardson, T. Matsuzaki, M. Murayama, E. Geslin and J.M. Bernhard, *Innovative TEM-coupled approaches to study foraminiferal cells.* Marine Micropaleontology, 2018. **138**: p. 90-104.
161. Kraft, M.L., P.K. Weber, M.L. Longo, I.D. Hutcheon and S.G. Boxer, *Phase separation of lipid membranes analyzed with high-resolution secondary ion mass spectrometry.* Science, 2006. **313**: p. 1948-1951.
162. Wirtz, T., Y. Fleming, U. Gysin, T. Glatzel, U. Wegmann, E. Meyer, U. Maier and J. Rychen, *Combined SIMS-SPM instrument for high sensitivity and high-resolution elemental 3D analysis.* Surface and interface analysis, 2013. **45**(1): p. 513-516.
163. Orphan, V.J., C.H. House, K.-U. Hinrichs, K.D. McKeegan and E.F. DeLong, *Methane-consuming Archaea revealed by directly coupled isotopic and phylogenetic analysis.* Science, 2001. **293**: p. 484-487.
164. Amann, R.I., L. Krumholz and D.A. Stahl, *Fluorescent-oligonucleotide probing of whole cells for determinative, phylogenetic, and environmental studies in microbiology.* Journal of Bacteriology, 1990. **172**(2): p. 762-770.
165. Pernthaler, A., J. Pernthaler and R. Amann, *Fluorescence In Situ Hybridization and Catalyzed Reporter Deposition for the Identification of Marine Bacteria.* Appl. Environ. Microbiol., 2002. **68**(6): p. 3094-3101.

166. Woebken, D., L.C. Burow, L. Prufert-Bebout, B.M. Bebout, T.M. Hoehler, J. Pett-Ridge, A.M. Spormann, P.K. Weber and S.W. Singer, *Identification of a novel cyanobacterial group as active diazotrophs in a coastal microbial mat using NanoSIMS analysis.* The ISME journal, 2012. **6**(7): p. 1427-1439.
167. Lemaire, R., R.I. Webb and Z. Yuan, *Micro-scale observations of the structure of aerobic microbial granules used for the treatment of nutrient-rich industrial wastewater.* ISME J, 2008. **2**(5): p. 528-541.
168. Hatzenpichler, R., S. Scheller, P.L. Tavormina, B.M. Babin, D.A. Tirrell and V.J. Orphan, *In situ visualization of newly synthesized proteins in environmental microbes using amino acid tagging and click chemistry.* Environmental microbiology, 2014. **16**(8): p. 2568-2590.
169. Bradley, J.P., Z.R. Dai, R. Erni, N.D. Browning, G.A. Graham, P.K. Weber, J.B. Smith, I.D. Hutcheon, H. Ishii, S. Bajt, C. Floss, F.J. Stadermann and S. Sandford, *An astronomical 2175 Å feature in interplanetary dust particles.* Science, 2005. **307**: p. 244-247.
170. Remusat, L., P.-J. Hatton, P.S. Nico, B. Zeller, M. Kleber and D. Derrien, *NanoSIMS study of organic matter associated with soil aggregates: advantages, limitations, and combination with STXM.* Environmental science & technology, 2012. **46**(7): p. 3943-3949.
171. De Samber, B., R. De Rycke, M. De Bruyne, M. Kienhuis, L. Sandblad, S. Bohic, P. Cloetens, C. Urban, L. Polerecky and L. Vincze, *Effect of sample preparation techniques upon single cell chemical imaging: A practical comparison between synchrotron radiation based X-ray fluorescence (SR-XRF) and Nanoscopic Secondary Ion Mass Spectrometry (nano-SIMS).* Analytica Chimica Acta, 2020.
172. Lehmann, J., J. Kinyangi and D. Solomon, *Organic matter stabilization in soil microaggregates: implications from spatial heterogeneity of organic carbon contents and carbon forms.* Biogeochemistry, 2007. **85**(1): p. 45-57.
173. Wan, J., T. Tyliszczak and T.K. Tokunaga, *Organic carbon distribution, speciation, and elemental correlations within soil microaggregates: applications of STXM and NEXAFS spectroscopy*. 2007.
174. Kopp, C., M. Wisztorski, J. Revel, M. Mehiri, V. Dani, L. Capron, D. Carette, I. Fournier, L. Massi and D. Mouajjah, *MALDI-MS and NanoSIMS imaging techniques to study cnidarian–dinoflagellate symbioses.* Zoology, 2015. **118**(2): p. 125-131.
175. Schlüter, S., T. Eickhorst and C.W. Mueller, *Correlative imaging reveals holistic view of soil microenvironments.* Environmental science & technology, 2018. **53**(2): p. 829-837.
176. Lin, S., S. Henze, P. Lundgren, B. Bergman and E.J. Carpenter, *Whole-Cell Immunolocalization of Nitrogenase in Marine Diazotrophic Cyanobacteria, Trichodesmium spp.* Appl. Environ. Microbiol., 1998. **64**(8): p. 3052-3058.
177. Levenson, R.M., A.D. Borowsky and M. Angelo, *Immunohistochemistry and mass spectrometry for highly multiplexed cellular molecular imaging.* Laboratory Investigation, 2015. **95**(4): p. 397-405.
178. Singer, S.W., C.S. Chan, M.H. Hwang, A. Zemla, N.C. VerBerkmoes, R.L. Hettich, J.F. Banfield and M.P. Thelen, *Characterization of Cytochrome579, an Unusual Cytochrome Isolated from an Iron-Oxidizing Microbial Community.* Applied and Environmental Microbiology, 2008. **74**: p. 4454-4462.

179. Gerard, E., F. Guyot, P. Philippot and P. Lopez-Garcia, *Fluorescence in situ hybridization coupled to ultra small immunogold detection to identify prokaryotic cells using transmission and scanning electron microscopy.* Journal of Microbiological Methods, 2005. **63**: p. 20-28.
180. Mayali, X., P.K. Weber, S. Mabery and J. Pett-Ridge, *Phylogenetic patterns in the microbial response to resource availability: amino acid incorporation in San Francisco Bay.* PlosOne, 2014. **9**(4): p. e95842.
181. Mayali, X., P.K. Weber and J. Pett-Ridge, *Taxon-specific C:N relative use efficiency for amino acids in an estuarine community.* FEMS Microbiology Ecology, 2013. **83**(2): p. 402-412.
182. Bryson, S., Z. Li, F. Chavez, P.K. Weber, J. Pett-Ridge, R.L. Hettich, C. Pan, X. Mayali and R.S. Mueller, *Phylogenetically conserved resource partitioning in the coastal microbial loop.* The ISME journal, 2017. **11**(12): p. 2781-2792.
183. Smith, D.F., A. Kiss, F.E. Leach, E.W. Robinson, L. Paša-Tolić and R.M. Heeren, *High mass accuracy and high mass resolving power FT-ICR secondary ion mass spectrometry for biological tissue imaging.* Analytical and bioanalytical chemistry, 2013. **405**(18): p. 6069-6076.
184. Steele, A.V., A. Schwarzkopf, J.J. McClelland and B. Knuffman, *High-brightness Cs focused ion beam from a cold-atomic-beam ion source.* Nano futures, 2017. **1**(1): p. 015005.

Figure Captions

Fig. 1. Correlated NanoSIMS nitrogen isotopic composition and TEM images of a *Trichodesmium* thin-section incubated for 8 hrs with ^{13}C-HCO_3^- and ^{15}N-N_2. The cyanobacterial filament was resin embedded, ultramicrotomed into 200 nm thick sections, imaged by TEM, and then analyzed by nanoSIMS. The nitrogen isotope data are shown as deviations from the natural abundance value in parts per thousand, as indicated in the legend ($\delta^{15}N$). Areas of ^{15}N enrichment indicate localization of newly fixed nitrogen, which is accumulated in cyanophycin granules (arrows) apparent in the TEM image. (Reprinted with permission from: Finzi-Hart, Pett-Ridge et al. *PNAS* 2008).

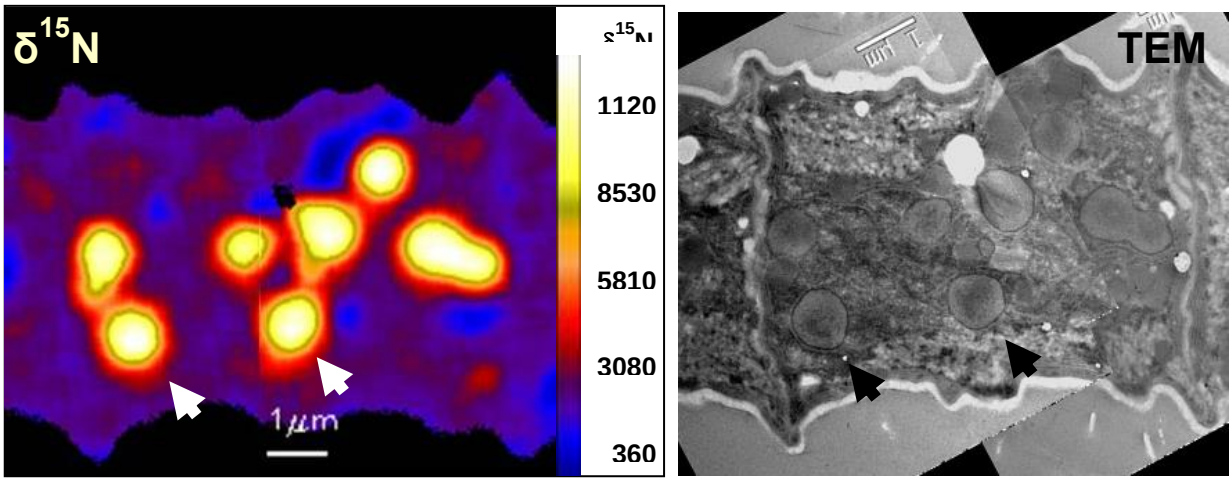

Fig 2. Thin section isotope imaging illustrates how newly acquired C and N is allocated to regions of active growth or maintenance. Correlated TEM and NanoSIMS images of a filamentous cyanobacterium, *Anabaena sp. SSM-00* (larger cells) infected by an epibiont (*Rhizobium* sp. WH2K) that attaches to the *Anabeana* heterocyst, the site of N fixation. The $\delta^{13}C$ and $\delta^{15}N$ images show that newly acquired ^{13}C and ^{15}N fixed by *Anabeana* is used by the epibiont, in addition to being allocated for active growth or maintenance in the *Anabeana.* Scale bar is 2µm. In collaboration with A. Spormann and W.O. Ng, Stanford University.

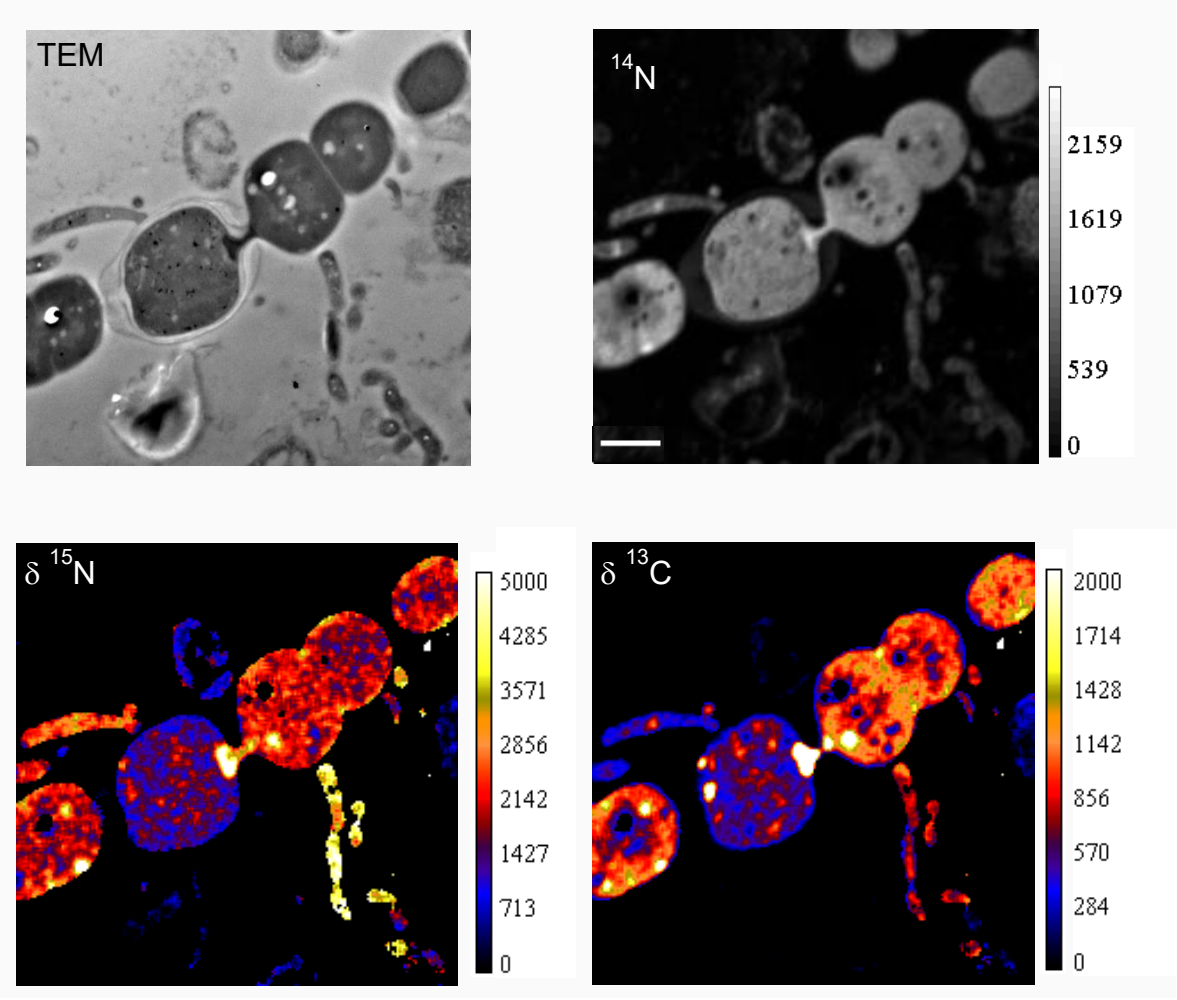

Fig. 3. TEM and NanoSIMS images illustrating the potential for analysis of subcellular elemental distribution in resin-embedded and microtome-sectioned cells. Top row, left to right: TEM of ultramicrotome section of mouse brain tissue, (a) a glial cell nucleus, (b) a blood vessel, and (c) myelinated axions are indicated; $^{12}C^{14}N^-$ ion image; $^{31}P^-$ ion image of the same region. (In collaboration with B. Anderson, SUNY Stony Brook). Bottom row, left to right: NanoSIMS secondary ion images showing the distributions of N (measured as CN^-) and P in sectioned non-Hodgkin's lymphoma cells (Raji). (In collaboration with G. L. DeNardo, University of California, Davis.)

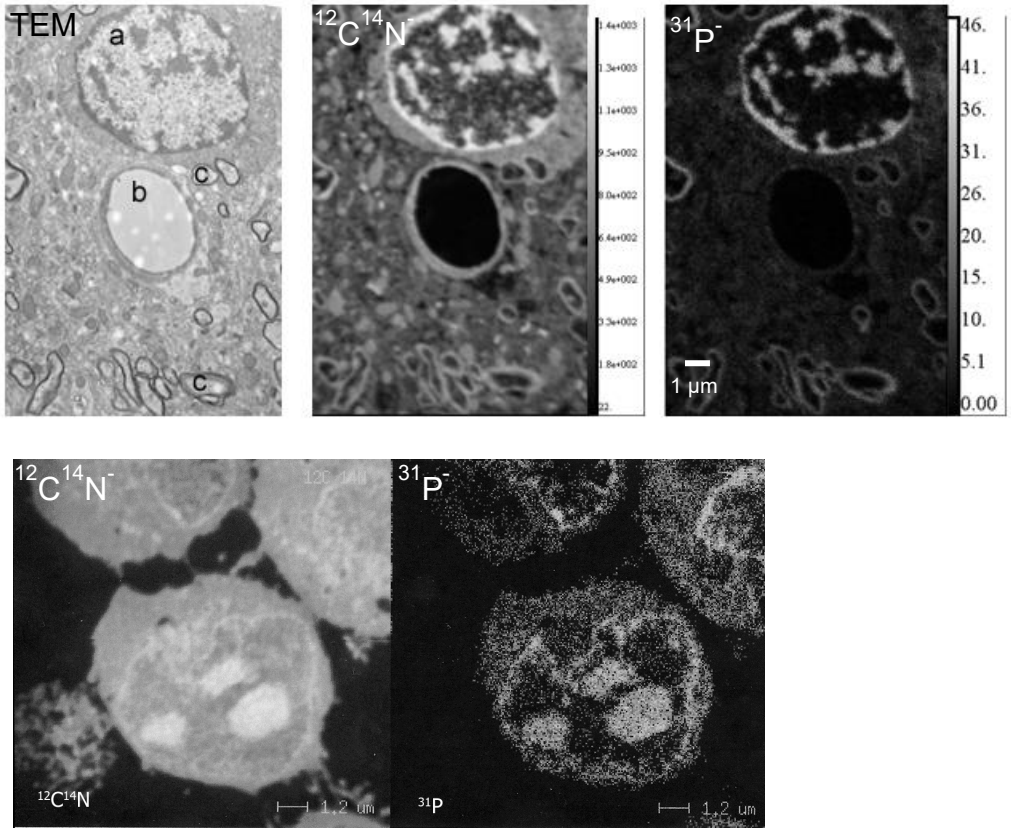

Fig. 4. (**i**) Zebrafish embryo retina sections for wild type (A, C, E & G) and copper deficient *Cal*^{gw71} embryos, (B, D, F, H). Left to right orientation is from inner to outer retina. A, B: Anatomical nuclear staining for reference. NanoSIMS images include: C, D: copper (Cu); E, F: phosphorous (P); G, H: overlay of copper and phosphorous images. GCL: Ganglion cell layer; IPL: Inner plexiform layer; INL: Inner nuclear layer; OPL: Outer plexiform layer; ONL: Outer nuclear layer; RPE: Retinal pigmented epithelium. Scale bar 25 μm. NanoSIMS copper ion image (D) for the copper deficient embryos show reduced copper in megamitochondria relative to the wild type in ONL, but elevated relative to other organs (not shown). These images provide evidence for copper prioritization for vision. **(ii)** Standard curve for copper generated by nanoSIMS analysis of matrix-matched standards plotted against copper concentrations determined by liquid ICP-MS. N ≥ 3 measurements per point. Error bars represent standard deviations. (Reprinted with permission from: Akerman et al. *Metallomics* 2018).

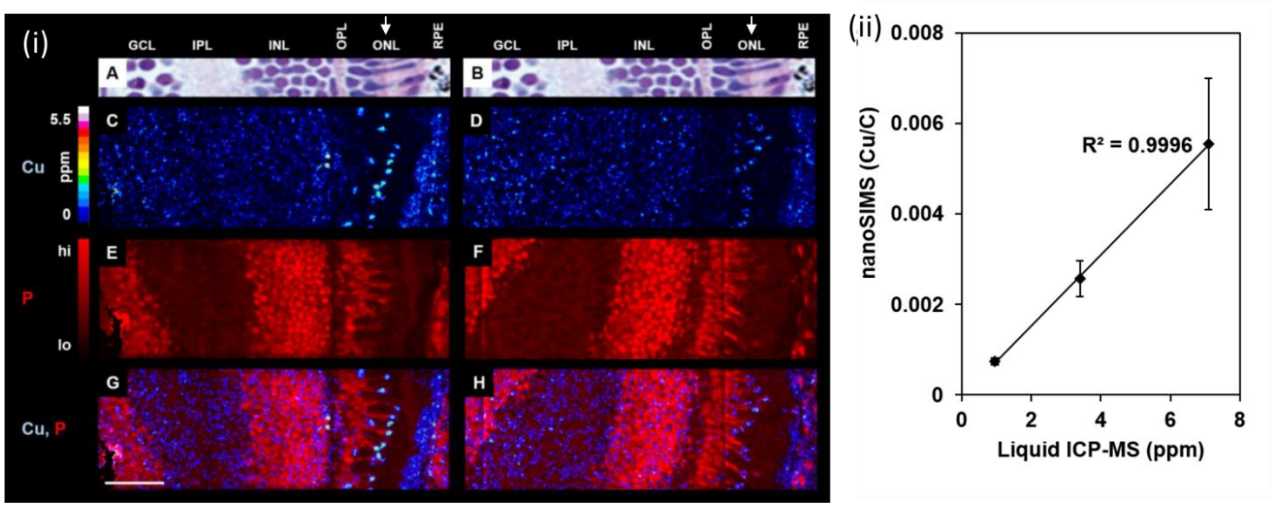

Fig. 5. NanoSIMS ion images showing co-localization of bromine ($^{77}Br^-$) with phosphorus ($^{31}P^-$) in a HeLa cell, indicating the incorporation of BrdU into DNA. The high P signal shows the location of the DNA in the nucleus. The lack of correlation between bromine and chlorine ($^{35}Cl^-$) indicates that the distribution of bromine is not the result of being a trace constituent in the major halide-bearing molecules. Results also showed the Br accumulates in the nucleus, suggesting that the DNA-RNA hybrid was being degraded. The cells were grown on a Si wafer, treated with BrdU, fixed and dried, and analyzed in the NanoSIMS by sputtering with high beam current until the nucleus was reached. (In collaboration with L. Dugan, LLNL).

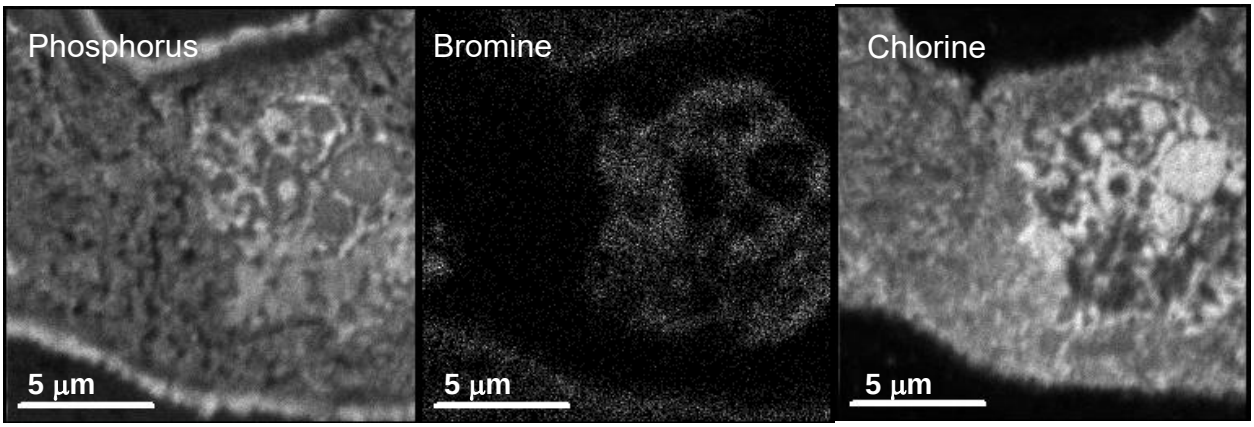

Fig. 6. (A) Chain of 5 cells from a filament of *A. oscillarioides* analyzed with NanoSIMS after 4 hours of incubation with $H^{13}CO_3^-$ and $^{15}N_2$. Het = Heterocyst. Individual cells are numbered to correspond with the numbering in part C. (A.1) = Image reconstruction based on secondary electrons. (A.2) = The distribution of ^{13}C enrichment. (A.3) = The distribution of ^{15}N enrichment. Enrichment is expressed as atom percent enrichment (APE). (B) = Post-analysis NanoSIMS secondary electron image of a filament of 50 cells of *A. oscillarioides* showing 3 heterocysts (Popa, 2007 #1969) after 4 h of incubation with $H^{13}CO_3^-$ and $^{15}N_2$. The white box indicates the area shown in the images A.1, A.2 and A.3. (C) = The cell-to-cell variation in ^{13}C (diamonds) and ^{15}N enrichment (squares) along the same 50 cells filament. There are 1 to 6 independent replicate measurements per cell. Error bars represent two standard errors (Reprinted with permission from: Popa et al. *ISME Journal* 2007).

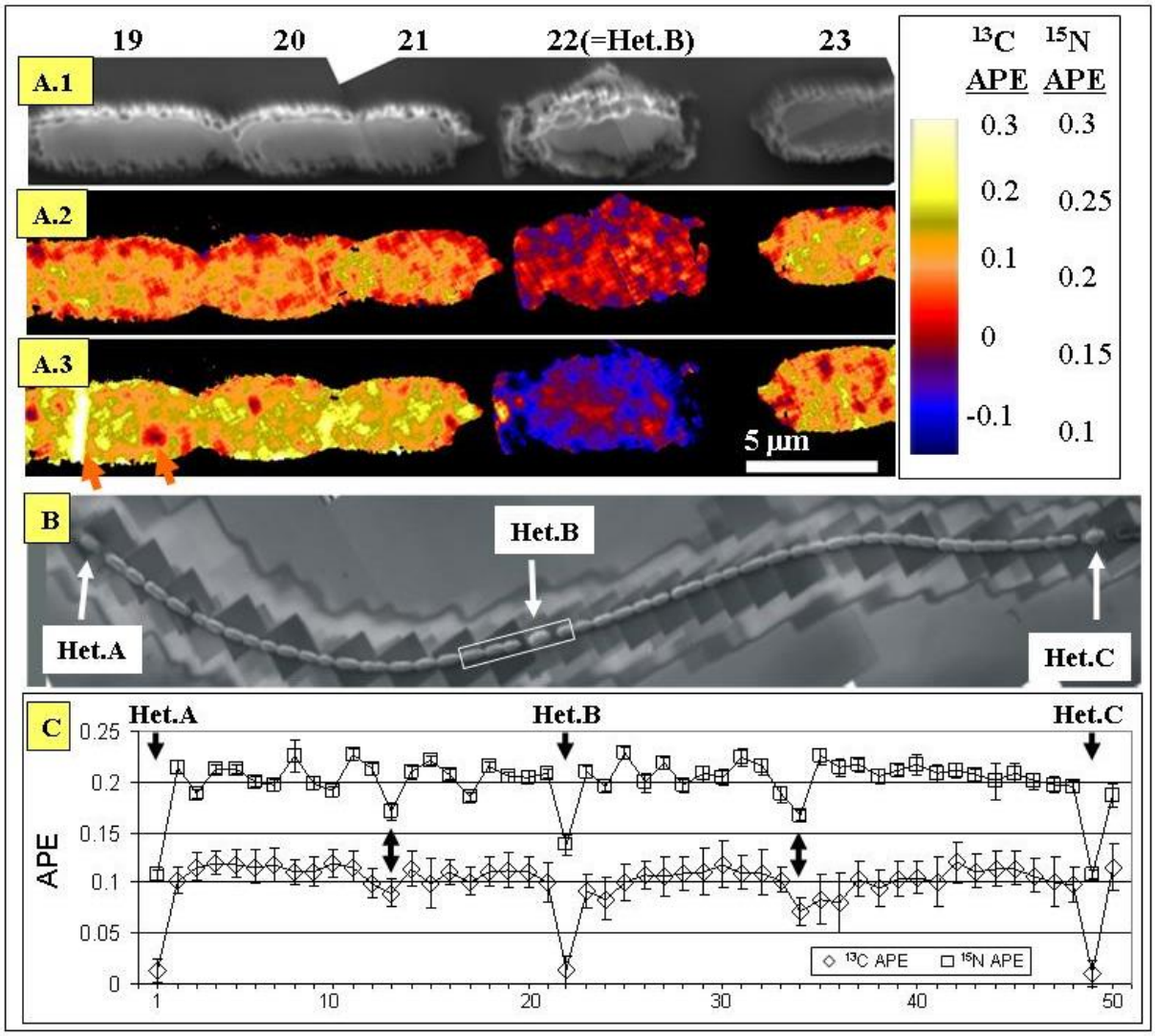

Fig. 7. Correlated SEM and NanoSIMS micrographs showing the localization of Rubisco, labeled with 5 nm immuno-gold in thin sections of the cyanobacterium *Trichodesmium* IMS 101. The immuno-gold can be image in the NanoSIMS, allow stable isotope probing and immuno-localization. Note that the gold enhances the production of CN- ions. (In collaboration with G. Sandh & B. Bergman, Stockholm University).

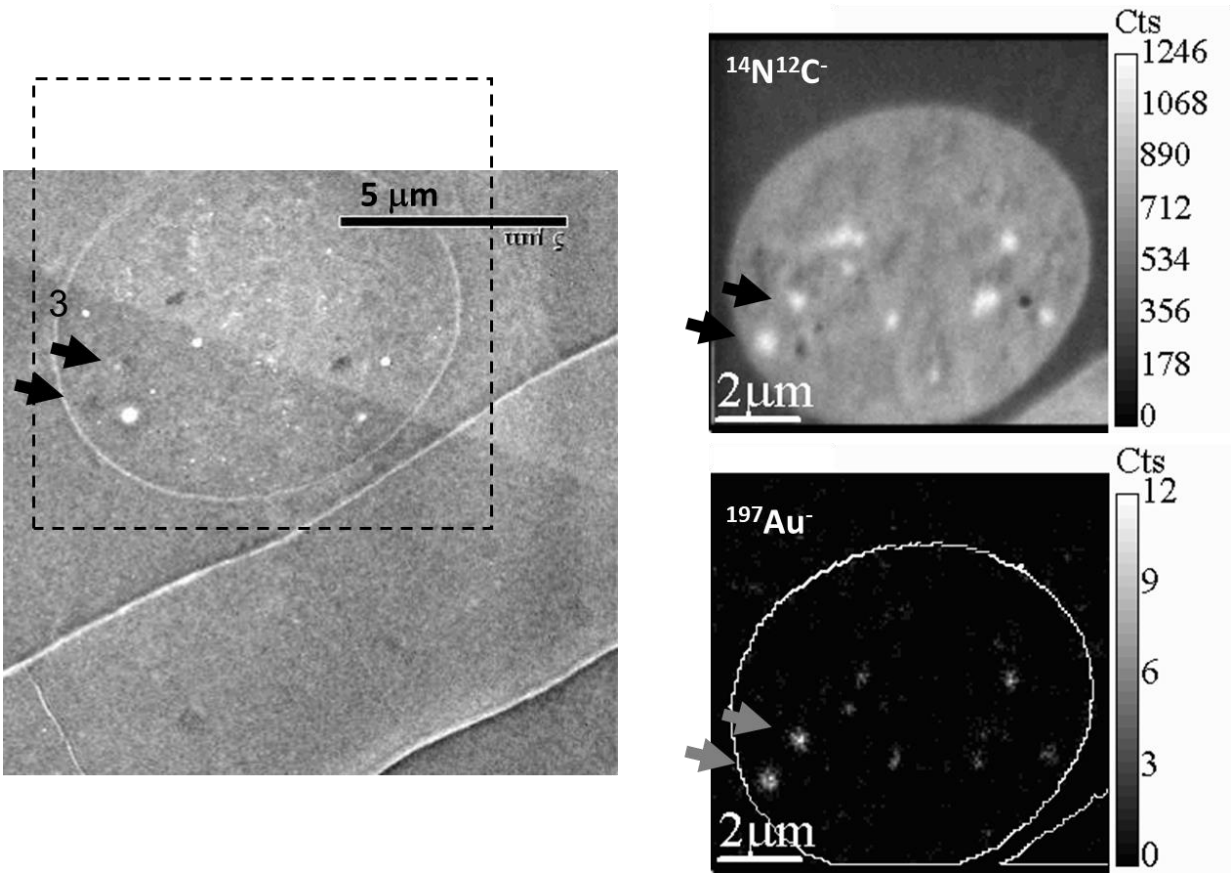

Fig. 8. Flattop peaks and ultimate precision. (a) Logarithmic and linear plots of a mass scan at mass 26. $^{12}C^{14}N^-$ is readily resolved from $H^{12}C^{13}C^-$, which is 0.007 amu heavier. $^{13}C_2^-$ is only 0.004 amu heavier than $^{12}C^{14}N^-$ and could be resolved, but typically is 4 to 5 orders of magnitude less abundant, and therefore is negligible. Note that the $^{12}C^{14}N^-$ peak is flat-topped, which means that a range of mass lines from the top of the peak can be aligned with the detector and precise measurements still be achieved. (b) Measurement precision is affected by instrument tuning and stability and sample characteristics, but the ultimate limit on measurement precision is the number of ions collected for the minor species. Therefore, in this example, the precision of the measurements of bacterial spores is lower than the precision for the graphite standard because the spores have less mass, and therefore less $^{13}C^-$ counts.

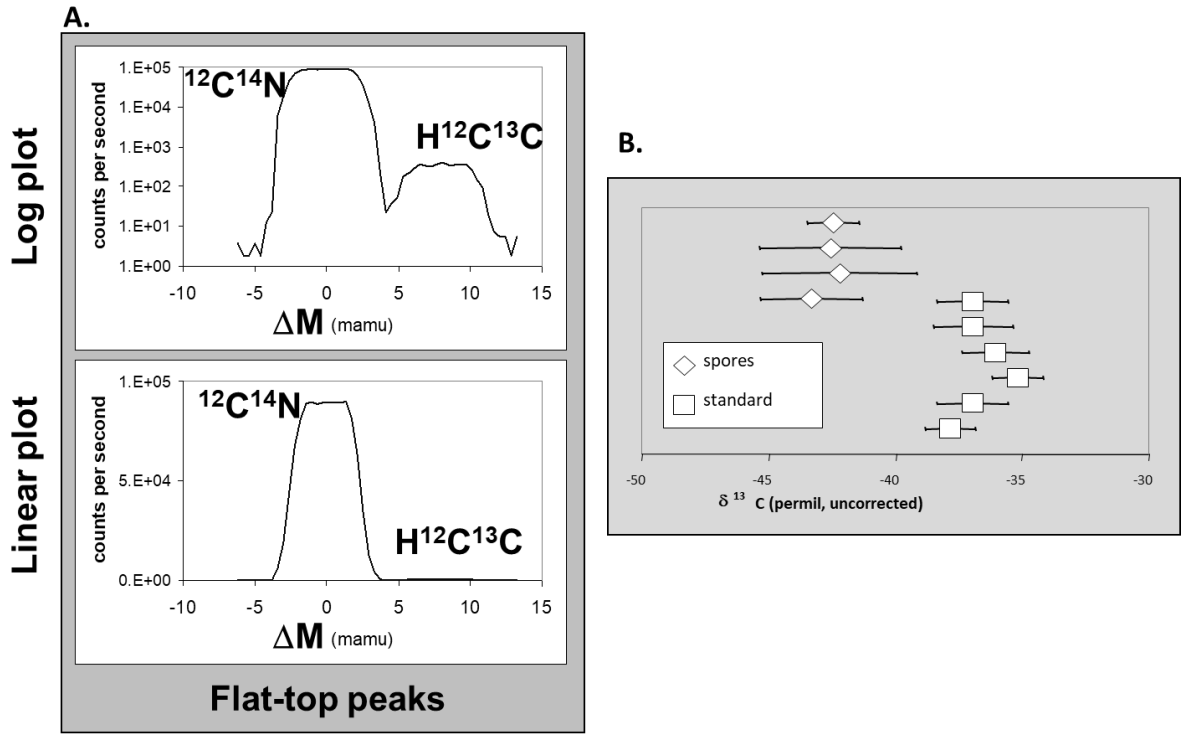

Fig. 9. NanoSIMS images of a filamentous cyanobacterium, *Anabaena sp. SSM-00* (larger cells) infected by an epibiont (*Rhizobium* sp. WH2K) that attaches to the *Anabeana* heterocyst, the site of N fixation. A and B are replicate filaments from the same culture, illustrating that cell to cell variation in isotopic enrichment may be extremely large, even while relative enrichment patterns remain consistent. (In collaboration with A. Spormann & W.O. Ng, Stanford University).

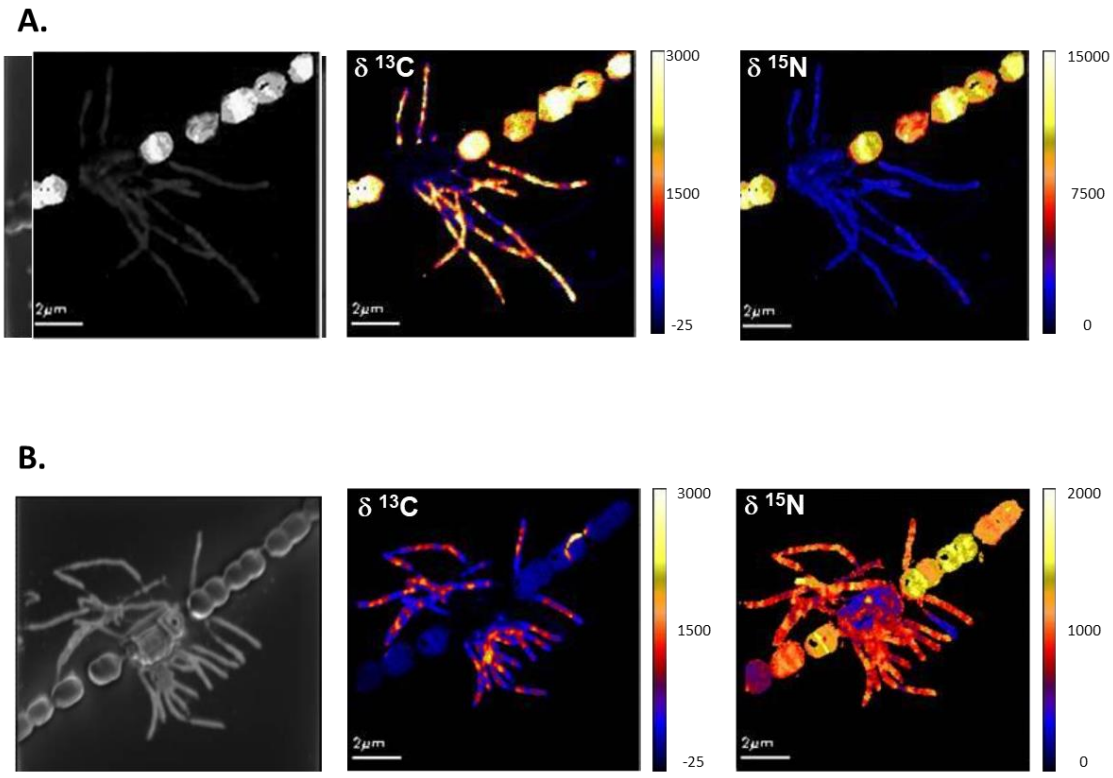

Fig. 10. Scan of the secondary ion beam focus voltage for lens E0S, showing the relative change in detected counts. The maximum transmission for $^{12}C^{14}N^-$ and $^{12}C_2^-$ coincide here, whereas the maximum transmission for $^{12}C^-$ is offset. While the $^{12}C^{14}N^-$ and $^{12}C_2^-$ scans are not always this well aligned, C is typically offset, resulting in either reduced transmission for C or CN if the two are detected simultaneously. The difference in count rate among these species varies from sample to sample, but in biological samples, CN typically has a higher count rate, and C and C_2 are similar.

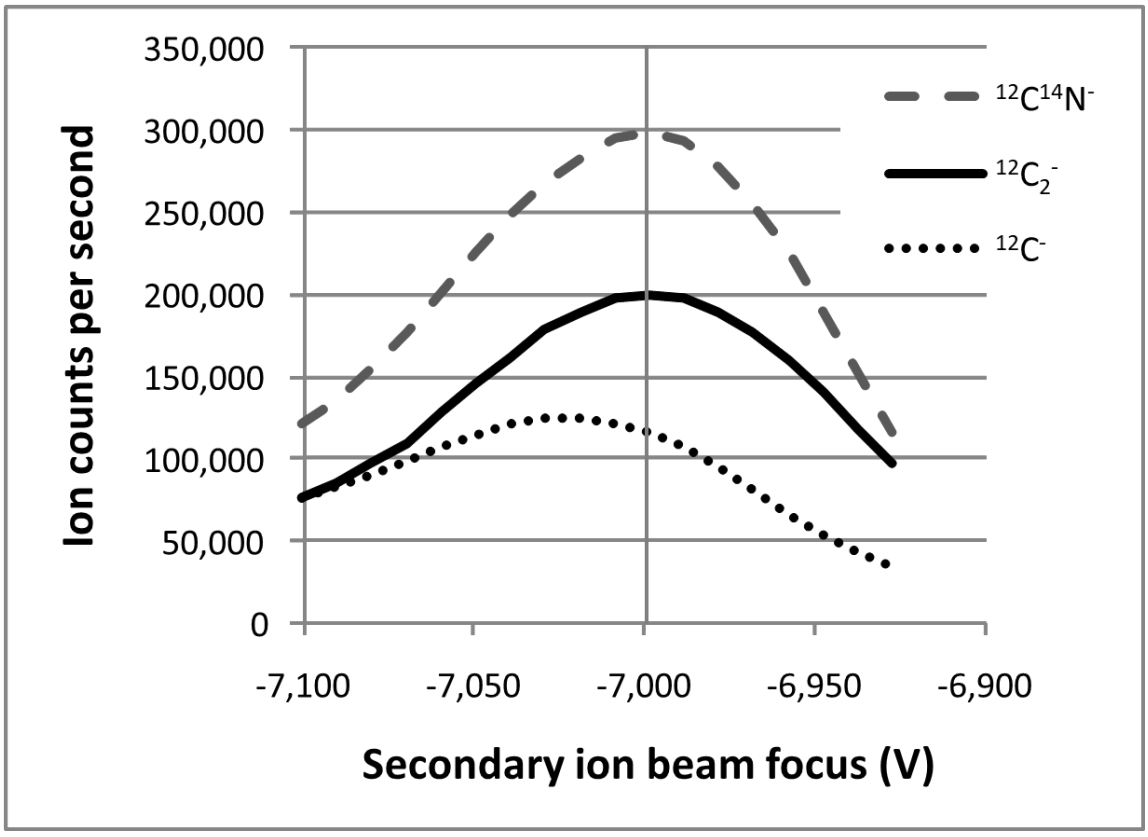

Fig. 11. Molybdenum distribution in an *Anabaena oscillarioides.* Filaments were fixed in gluteraldehyde and sputtered with O^- beam to a depth of 1µm on a Si planchette (wafer). Data for multiple Mo isotopes were collected to assess for isobaric interferences. Top: ion ratio map of $^{98}Mo^-$ normalized to $^{12}C^-$ for quantification. A thin white line outlines each individual cell. Grey triangles indicate heterocyst cells. Bottom: data summary for two replicate filaments. Heterocyst cells are consistently enriched in Mo, a critical nitrogenase co-factor, suggesting active N-fixation. Mo concentrations are estimates based on published relative sensitivity factors (Wilson, 1989). Mean Mo concentration is 64 (±4) µg/g in heterocysts (n = 5) and 18 (±0.9) µg/g in vegetative cells (n = 46).

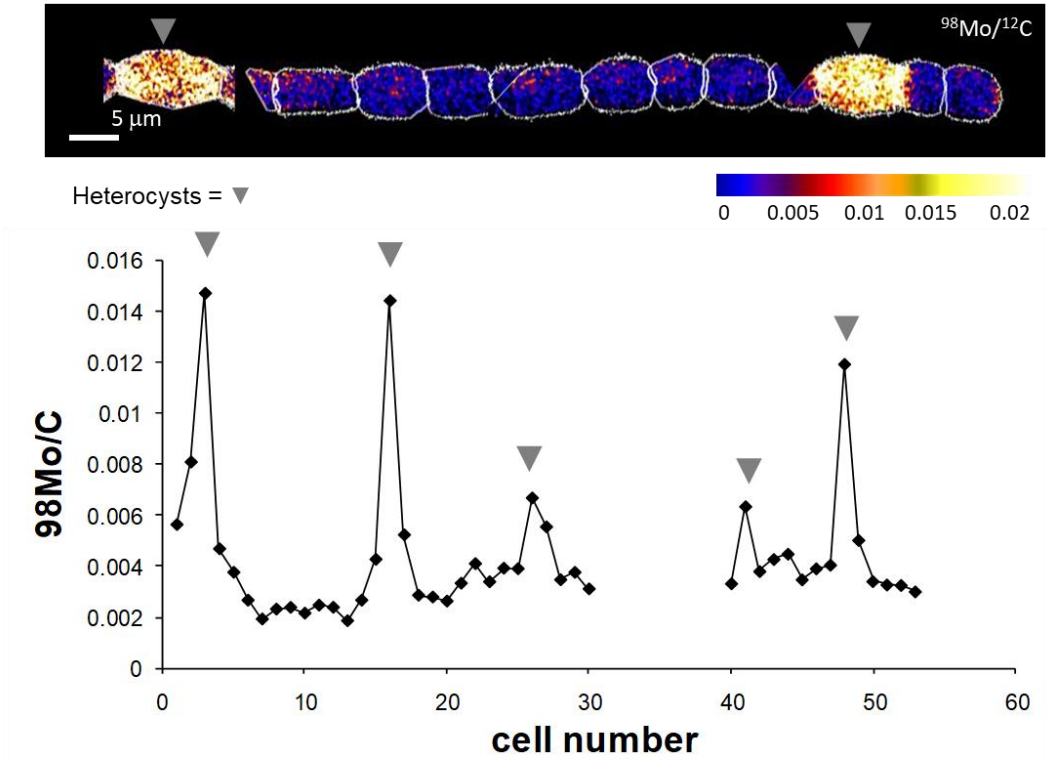

Fig. 12. Representative nanoSIP images demonstrating high-throughput metabolic screening of cells filtered from Pacifica, California seawater incubated with ^{13}C-bicarbonate and ^{15}N-amino acids for 6 days. $^{14}N^{12}C^-$ ion counts reflect all carbon- and nitrogen-containing particles, ^{13}C atom percent indicates cells enriched in ^{13}C, and ^{15}N atom percent indicates cells enriched in ^{15}N. The same four cells are indicated with arrows in each panel, with letters in the first panel indicating putative metabolism: I (no enrichment; inactive cell), C1 (enrichment in only ^{13}C; chemoautotroph), H (enrichment in only ^{15}N; heterotroph), and C2, (enrichment in ^{13}C, minor enrichment in ^{15}N; chemoautotroph). Scale bar is 11 μm. (Reprinted with permission from: Dekas et al. *Frontiers in Microbiology* 2019).

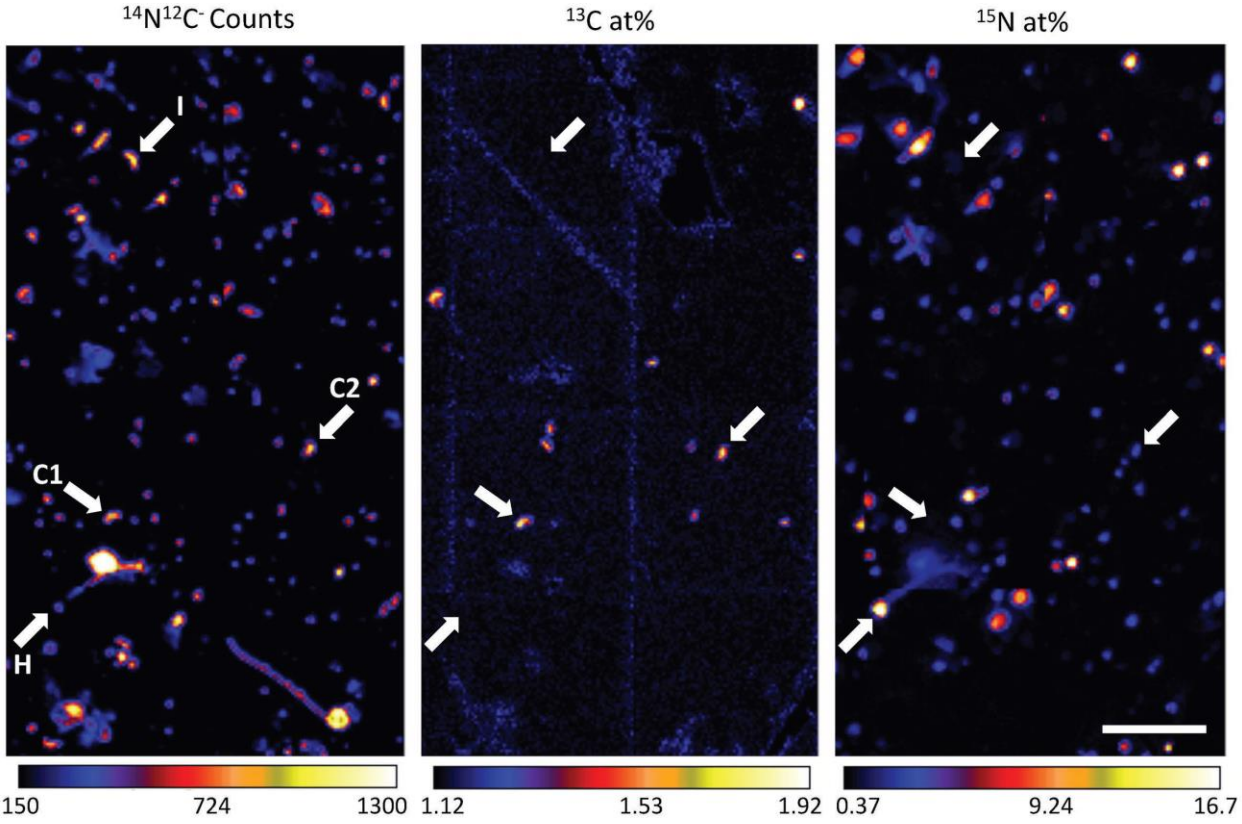

Fig. 13. Comparison of NanoSIMS-based characterization of sectioned versus whole *Bacillus thuringiensis* (*Bti*) spores. (A) TEM image of a sectioned *Bti* spore showing its layered architecture and overall dimensions. Scale bar 200 nm. (B) Lateral profile across the surface of a sectioned *Bti* spore showing the distribution of ^{12}C, ^{31}P, and ^{35}Cl. The dashed lines identify the core region based on the ^{31}P profile. The whole spore is defined based on the ^{12}C profile and identified by solid lines. Profile: length 1200 nm; width 200 nm. (C) Model representation of a sectioned spore with the highlighted rectangular region representing the location of profile data. (D-F) NanoSIMS secondary ion images showing the distribution of ^{12}C, ^{31}P, and ^{35}Cl across the sectioned spore surface. Scale bar 200 nm. (G) SEM image of a whole *Bti* spore. Scale bar 200 nm. (H) Depth profile of whole spore showing the distribution of ^{12}C, ^{31}P, and ^{35}Cl as a function of depth in the spore. (I) Model representation of a whole spore with the highlighted column representing the location of the profile data. Profile diameter 200 nm. (J-L) NanoSIMS secondary ion images showing the spatial distribution of ^{12}C, ^{31}P, and ^{35}Cl in the spore. Scale bar 500 nm. Both profiles were acquired with the Cs^{22} primary ion beam. (Reprinted with permission from: Ghosal et al. *Analytical Chemistry* 2008).